Article

Current Biology

Discovery of a novel flagellar filament system underpinning *Leishmania* adhesion to surfaces

Highlights

- *Leishmania* has a set of filament bundles in the proximal region of the flagellum
- Kinetoplastid-insect adhesion protein 2 (KIAP2) is a key component of the filaments
- The flagellum attachment zone remodels during parasite adhesion
- The flagellum attachment zone is important for stable parasite adhesion

Authors

Barrack O. Owino, Ryuji Yanase, Alan O. Marron, Flavia Moreira-Leite, Sue Vaughan, Jack D. Sunter

Correspondence

jsunter@brookes.ac.uk

In brief

Leishmania adhere to substrates through a modified flagellum. Owino et al. identify a novel set of filament bundles in the proximal region of the *Leishmania* flagellum and show that kinetoplastid-insect adhesion protein 2 (KIAP2) is a key component of these filaments. Additionally, they show the flagellum attachment zone is important for adhesion.

Owino et al., 2025, Current Biology *35*, 2837–2847
June 23, 2025
https://doi.org/10.1016/j.cub.2025.04.064

CellPress

Current Biology

CellPress
OPEN ACCESS

Article

Discovery of a novel flagellar filament system underpinning *Leishmania* adhesion to surfaces

Barrack O. Owino,[1] Ryuji Yanase,[1,2,3] Alan O. Marron,[1] Flavia Moreira-Leite,[1,4] Sue Vaughan,[1] and Jack D. Sunter[1,5,*]
[1]Oxford Brookes University, Department of Biological and Medical Sciences, Gipsy Lane, Oxford OX3 0BP, UK
[2]Present address: University of Nottingham, School of Life Sciences, Queen's Medical Centre, Nottingham NG7 2UH, UK
[3]Present address: University of Leicester, Department of Genetics and Genome Biology, University Road, Leicester LE1 7RH, UK
[4]Present address: University of Oxford, Department of Biochemistry, Central Oxford Structural Molecular Imaging Centre (COSMIC), South Parks Road, Oxford OX1 3QU, UK
[5]Lead contact
*Correspondence: jsunter@brookes.ac.uk
https://doi.org/10.1016/j.cub.2025.04.064

SUMMARY

Adhesion to surfaces is a common strategy employed across biology, especially by pathogens. Within their sand fly vector, *Leishmania* parasites undergo multiple developmental stages, including the understudied haptomonad form, which adheres to the sand fly stomodeal valve via a highly modified flagellum. This adhesion, likely critical for efficient transmission, is mediated by a complex adhesion plaque from which filaments in the modified flagellum extend toward the cell body and likely connect to the flagellum attachment zone (FAZ), a cytoskeletal structure important for cell morphogenesis. However, the role of the FAZ in adhesion and its relationship with the kinetoplastid-insect adhesion proteins (KIAPs) and the filamentous structures of the plaque itself remain unclear. Here, to examine the role of the FAZ in adhesion, we generated FAZ2, FAZ5, and FAZ34 deletion mutants. Deletion of any of these FAZ proteins impaired parasite adhesion *in vitro*. Furthermore, we identified a novel and distinct set of extra-axonemal flagellar filaments important for adhesion and demonstrated that KIAP2 is an essential component of these filaments. Our findings underscore the importance of a robust connection from the cell body to the adhesion plaque for stable *Leishmania* adhesion via the highly modified flagellum.

INTRODUCTION

A common approach of pathogens to avoid clearance and promote transmission is to anchor themselves to tissues and surfaces. *Yersinia pestis*, the plague bacterium, is a well-studied example, as it proliferates in the gut of the flea as an attached biofilm.[1] The unicellular eukaryotic parasite *Leishmania* also adopts this strategy in its insect vector. *Leishmania* spp. are protozoan parasites transmitted by an infected sand fly and are of public health importance as the causative agents of leishmaniasis. Leishmaniasis has a broad geographic distribution, affecting approximately 700,000 to 1 million people worldwide annually,[2] with a range of clinical symptoms from disfiguring skin lesions to severe infections of the internal body organs.[3–5] There are few drugs to treat leishmaniasis, most of which have severe side effects, and overreliance on them has led to a global increase in drug resistance.[6]

Leishmania has a complex life cycle, with distinct morphological forms as it cycles between a vertebrate host and a sand fly vector.[7–10] In the sand fly, the parasite undergoes multiple developmental stages, including motile and adhered forms. The promastigote forms are motile, with an elongated cell body and long flagellum.[8] The adhered forms include the nectomonad form, which transiently adheres to the microvilli of the midgut, and the haptomonad form that stably adheres to the cuticular lining of the stomodeal valve.[9,11–14] Haptomonad adhesion to the stomodeal valve contributes to *Leishmania* transmission through two interconnected phenomena. First, haptomonads contribute to promastigote secretory gel production that, along with the damage adhesion causes to the stomodeal valve, results in more frequent but incomplete sand fly feeding.[8,13,15–17] Second, haptomonads can undergo asymmetric division to generate free-swimming promastigote forms, contributing to persistent infections in the sand fly.[18] Moreover, recent work has shown that detached haptomonads are infective in their own right.[14]

The promastigote morphology of the free-swimming *Leishmania* parasite is characterized by the positioning of the mitochondrial DNA (kinetoplast) to the anterior of the nucleus, with a long motile flagellum emerging from the anterior cell tip (Figure 1A). The flagellum is assembled from the basal body, which is physically connected to the kinetoplast. There is an invagination of the cell membrane around the base of the flagellum called the flagellar pocket, which is made up of a bulbous domain proximal to the kinetoplast and a flagellar pocket neck domain extending to the anterior cell tip in which the membrane of the cell body is close to the flagellum. Along one side of the flagellar pocket neck, the flagellum cytoskeleton is laterally connected to the cell body cytoskeleton through the cell body and flagellum membranes by a complex

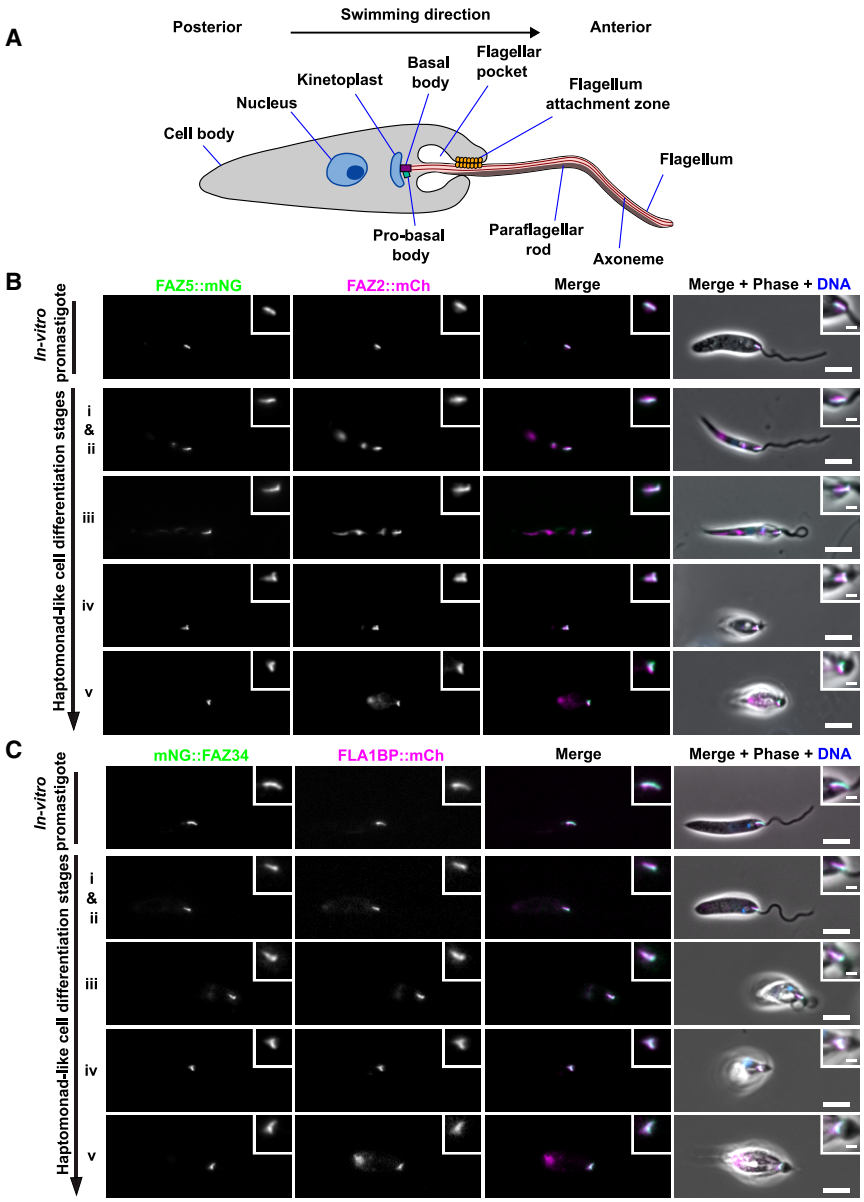

Figure 1. FAZ undergoes structural modification during differentiation of *in vitro L. mexicana* promastigote to haptomonad-like cells

(A) Schematic of the *Leishmania* promastigote cell morphology aligned along the posterior-anterior axis with key structures in the flagellum indicated. (B and C) Fluorescence micrographs of *in vitro L. mexicana* promastigote and haptomonad-like cells at different differentiation stages (i–v) expressing mNeonGreen (mNG; green)- or mCherry (mCh; magenta)-tagged FAZ proteins from the cell body (FAZ2), intermembrane (FAZ5 and FLA1BP), and flagellum (FAZ34) domains, *in situ*. DNA was stained with Hoechst 33342 (blue). (B) FAZ5 and FAZ2 and (C) FAZ34 and FLA1BP. The insets at the top right corner of each image illustrate the details of the FAZ localization. The fluorescence intensities were adjusted to show the shape of the FAZ signal. Scale bars, 5 μm; insets, 1 μm.
See also Figure S1.

cytoskeletal structure called the flagellum attachment zone (FAZ)[19,20] (Figure 1A).

The FAZ is organized into three major domains (cell body, intermembrane, and flagellum domains), and FAZ proteins that localize to each domain have been identified.[21,22] Studies of these proteins have shed light on the functional significance of the FAZ in *Leishmania* biology.[19,20,22,23] FAZ5, a key component of the intermembrane domain, was shown to be essential for maintaining flagellar pocket architecture, with null mutants unable to develop late-stage infections in the sand fly and having reduced virulence in mice.[20] Further, the deletion of FAZ2, a component of the cell body FAZ domain, disrupted the anterior cell tip morphogenesis, resulting in FAZ-mediated flagellum-to-flagellum connections.[19] FAZ7B, which localizes to the cell body domain of the FAZ, is also important for cell division and morphogenesis.[23] We have also shown that FAZ34, which localizes to the FAZ flagellum domain, is required for flagellum attachment to the *Leishmania* cell body, with FAZ34 deletion resulting in flagellum loss and altered anterior cell tip morphology.[22] Collectively, these findings demonstrate the importance of the FAZ for the morphogenesis of the flagellar pocket and anterior cell tip, which impacts on the pathogenicity and life cycle progression of the parasite.

We have shown that promastigote differentiation to *in vitro* haptomonad-like cells proceeds through five steps, from initial adhesion at any point along the flagellum, followed by disassembly of the flagellum, to final haptomonad maturation.[18] Furthermore, earlier work and our recent three-dimensional ultrastructural analysis have shown that haptomonad adhesion is mediated by a highly modified, shortened flagellum.[18,24] Ultimately, at the interface of the flagellum and the underlying stomodeal valve, a complex adhesion plaque forms that connects to the surface of the stomodeal valve, with a filamentous network extending from the plaque toward the *Leishmania* cell body and the FAZ. We have identified three kinetoplastid-insect adhesion proteins (KIAP1–3), which localize to the adhered haptomonad flagellum and are essential for parasite adhesion.[15] Yet the relationship between the cell body FAZ domain and the distal plaque region defined by KIAP1 and KIAP3 is unclear.

Here, we discovered a new set of extra-axonemal flagellar filaments as the flagellum emerged from the cell body and show that KIAP2 is an essential component of them. Deletion of either FAZ2, FAZ5, or FAZ34 impaired *Leishmania* adhesion *in vitro*, and in the latter mutant there was a disconnection of the KIAP2-containing filaments from the anterior cell tip, causing a cell body mispositioning relative to the adhesion plaque and a

smaller plaque size with lower levels of KIAP1 and 3 when compared with the parental cells. Overall, this demonstrates that stable parasite adhesion requires a connection from the cell body through to the adhesion plaque.

RESULTS

The FAZ is modified during differentiation to *in vitro* haptomonad-like cells

We have shown by serial electron tomography that there are ultrastructural changes to the anterior cell tip during haptomonad differentiation, including changes to the organization of the FAZ.[18] To understand the changes in FAZ protein localization occurring during differentiation to *in vitro* haptomonad-like cells, we generated cell lines expressing mNeonGreen (mNG) and mCherry (mCh)-tagged FAZ proteins characteristic of the different FAZ domains—cell body (FAZ2), intermembrane (FAZ5 and FLA1BP), flagellum (FAZ34), and flagellum exit point (FAZ10)—and examined their localization in cells at different stages of haptomonad differentiation. In the non-adhered promastigotes, all the tagged proteins, except FAZ10, localized as a short line within the flagellar pocket neck region, with FAZ2 and FAZ5 in the cell body and FLA1BP and FAZ34 within the flagellum (Figures 1B and 1C). FAZ10 localized as a ring at the flagellum exit point from the cell body (Figure S1A). During differentiation to haptomonad-like cells, there was a change to the shape of the fluorescence signal of FAZ2, FAZ5, FLA1BP, and FAZ34 (Figures 1B and 1C). As differentiation progressed, there was an elaboration of the fluorescence signal, with additional lobes seen at the anterior cell tip generating an L- or Y-shaped appearance (stages iii and iv). During the final stages of differentiation, the line parallel to the flagellar pocket neck shortened until the only observable tagged FAZ protein signal was from the anterior cell tip to give a C-shaped signal in mature (stage v) haptomonad-like cells. In contrast, FAZ10 maintained its ring shape throughout the differentiation process (Figure S1A). These data provide further evidence that the FAZ undergoes structural modifications during haptomonad differentiation.

Next, we examined the positioning of the FAZ relative to KIAP1–3 using cell lines expressing mNG::FAZ34 and KIAP1::mCh, KIAP2::mCh, or mCh::KIAP3. We focused on FAZ34 because it is found in the flagellum domain of the FAZ[22] and was likely to be positioned closer to the adhesion plaque. In the *in vitro* haptomonad-like cells, mNG::FAZ34 localized with a C-shaped signal and was positioned adjacent to the enlarged region of the adhered flagellum, with the signals from KIAP1–3 concentrated in this region (Figures S1B and S1C). Notably, FAZ34 localized more closely to KIAP2 than KIAP1 and KIAP3 in the adhered haptomonad-like cells (Figure S1C).

FAZ2, FAZ5, and FAZ34 are required for haptomonad-like cell adhesion *in vitro*

Given the localization changes of key FAZ proteins during *in vitro* haptomonad-like cell differentiation, we asked whether these FAZ proteins could be important for haptomonad-like cell adhesion. To investigate this, previously generated FAZ2, FAZ5, and FAZ34 deletion mutants and add-back cell lines[19,20,22] were allowed to adhere on gridded glass coverslips for 24 h and the numbers of adhered cells compared with those of the parental cells (Figures 2A and 2B). The growth rate of the FAZ2, FAZ5, and FAZ34 null mutants as *in vitro* promastigotes was unaffected (Figure S2A). However, there was a significant reduction in the number of adhered cells for each of the FAZ null mutants, although the add-back of FAZ2 and FAZ34 restored the ability of the parasites to adhere (Figure 2B). We saw little recovery of adhesion in our initial assays with the FAZ5 add-back cell line (Figure S2B). In this cell line, the FAZ5 protein was fused to mCh, and we therefore decided to generate an FAZ5 add-back cell line in which the FAZ5 protein was unmodified. We confirmed the presence of the FAZ5 open reading frame by PCR (Figure S2C). There was an increase in parasite adhesion when using this FAZ5 add-back cell line compared with the FAZ5 null mutant (Figure 2B). Together, this shows that FAZ2, FAZ5, and FAZ34 are required for adhesion of haptomonad-like cells to substrates.

FAZ34 is required for the integration of KIAP1 and KIAP3 into the adhesion plaque

Given the position of FAZ34 within the flagellum FAZ domain and its effect on adhesion, we asked whether the loss of FAZ34 impaired the localization of KIAP1-3 to the adhered flagellum. To address this, we endogenously tagged KIAP1–3 with mNG in the parental and FAZ34 deletion mutants, allowed the cells to adhere to glass coverslips for 24 h, and compared the fluorescence intensities of tagged KIAP1–3 signal in the adhered flagellum of mature parental and FAZ34 null mutant haptomonad-like cells. After adhesion, KIAP1, KIAP2, and KIAP3 localized in the expanded region of the flagellum of both the parental and FAZ34 null mutant (Figure 3A). There was a significantly reduced signal in the FAZ34 null mutant compared with the parental cells for both KIAP1 and KIAP3, whereas KIAP2 signals were similar between the cell lines (Figures 3A and 3B).

Using super-resolution confocal microscopy, we investigated the effect of the decreased amount of KIAP1 and KIAP3 on the size of the adhesion plaque. We generated parental and FAZ34 null mutant cell lines expressing SMP1 endogenously tagged with mCh, as SMP1 is a flagellum membrane marker and is excluded from the adhesion plaque membrane.[15] Then, we measured the area of the space bound by the SMP1 signal in mature parental and FAZ34 null mutant haptomonad-like cells. The area enclosed by the SMP1 signal was significantly smaller in the FAZ34 null mutants than in the parental cells (Figures S3A and S3B). Overall, this shows that FAZ34 is required for correct adhesion plaque assembly.

FAZ34 deletion disconnected KIAP2 and a novel set of filaments from the promastigote anterior cell tip

When we examined our images of mNG-tagged KIAP2 in non-adhered FAZ34 null mutant promastigote cells, we observed a gap separating KIAP2 signal from the anterior cell tip (Figure 4A). To investigate the changes at the anterior cell tip in the FAZ34 null mutants, we measured the distance between the kinetoplast and the anterior cell tip, as a measure of correct anterior cell tip morphogenesis,[19,20,22] and the distance between the kinetoplast and the proximal end of the KIAP2::mNG signal. The distance between the kinetoplast and the anterior cell tip was significantly shorter in the FAZ34 null mutant than in the parental cells (Figure 4B), as previously observed,[22] although the position

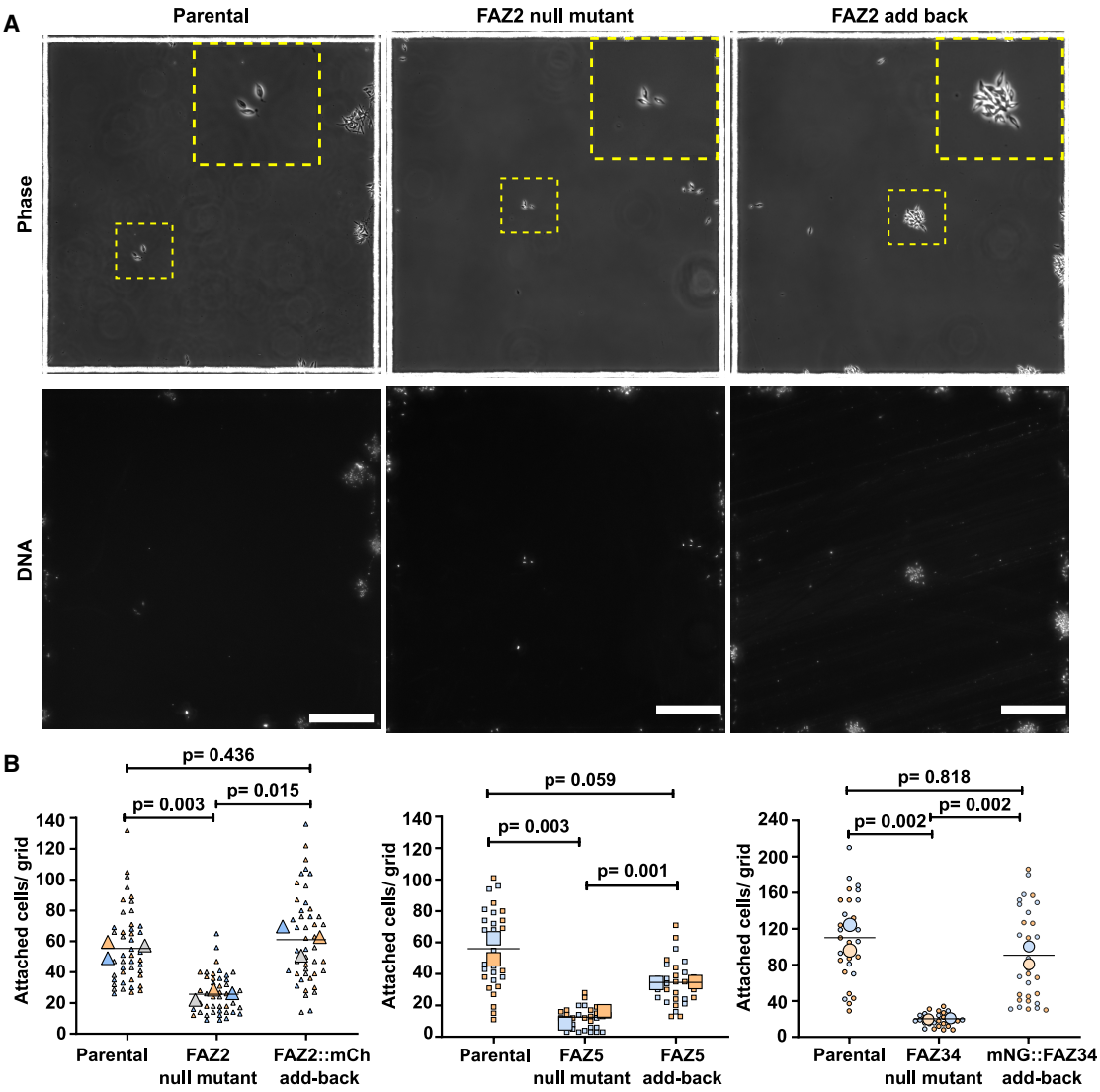

Figure 2. FAZ2, FAZ5, and FAZ34 are required for adhesion of haptomonad-like cells *in vitro*

(A) Phase and Hoechst fluorescence micrographs of *L. mexicana* parental, FAZ2 null mutant, and FAZ2::mCh add-back after 24 h of induced haptomonad differentiation on gridded glass coverslips. Representative images of adhered cells per grid area are shown for FAZ2 parental, null mutant, and add-back cell lines. Top: phase contrast images. Bottom: Hoechst 33342-stained DNA. Insets show a magnified view of the yellow-dotted squares, illustrating examples of adhered cells per cell line. Scale bars, 100 μm.

(B) Quantification of the number of adhered cells per grid for FAZ2 (left), FAZ5 (middle), and FAZ34 (right) parental deletion mutants and add-back *L. mexicana* cell lines. The blue, orange, and gray colors represent measurements from three (for FAZ2) or two independent experiments (for FAZ5 and FAZ34). The small triangles, squares, or circles indicate counts per grid area, whereas the large ones show the mean values per experiment. The horizontal bars represent the overall mean values of adhered cells per grid area across the experiments. The *p* values for FAZ2 and FAZ5 data were calculated using two-tailed Welch's t test, whereas those of FAZ34 data were determined using the Mann-Whitney test.

See also Figure S2.

of the KIAP2::mNG signal did not change relative to the kinetoplast (Figure 4C). This suggests that the position of KIAP2 is dependent on a flagellum-, but not cell-body-based, mechanism.

We asked whether there was a structure responsible for maintaining KIAP2 protein at this specific point in the proximal region of the flagellum. To address this, we examined negatively stained parental and FAZ34 null mutant detergent-extracted cytoskeletons by transmission electron microscopy (TEM), enabling us to observe the cytoskeletal structures of the flagellum without the flagellum membrane and cytoplasm. This revealed sets of hitherto undescribed filament bundles on the axoneme as it emerged from the cell body (Figure 4D). The filaments generally lay parallel to the axoneme, on the opposite side to the paraflagellar rod (PFR), a complex, extra-axonemal structure that runs alongside the axoneme.[25,26] In the parental cells the filaments were positioned adjacent to the anterior cell tip, with no clear gap between the anterior cell tip and the

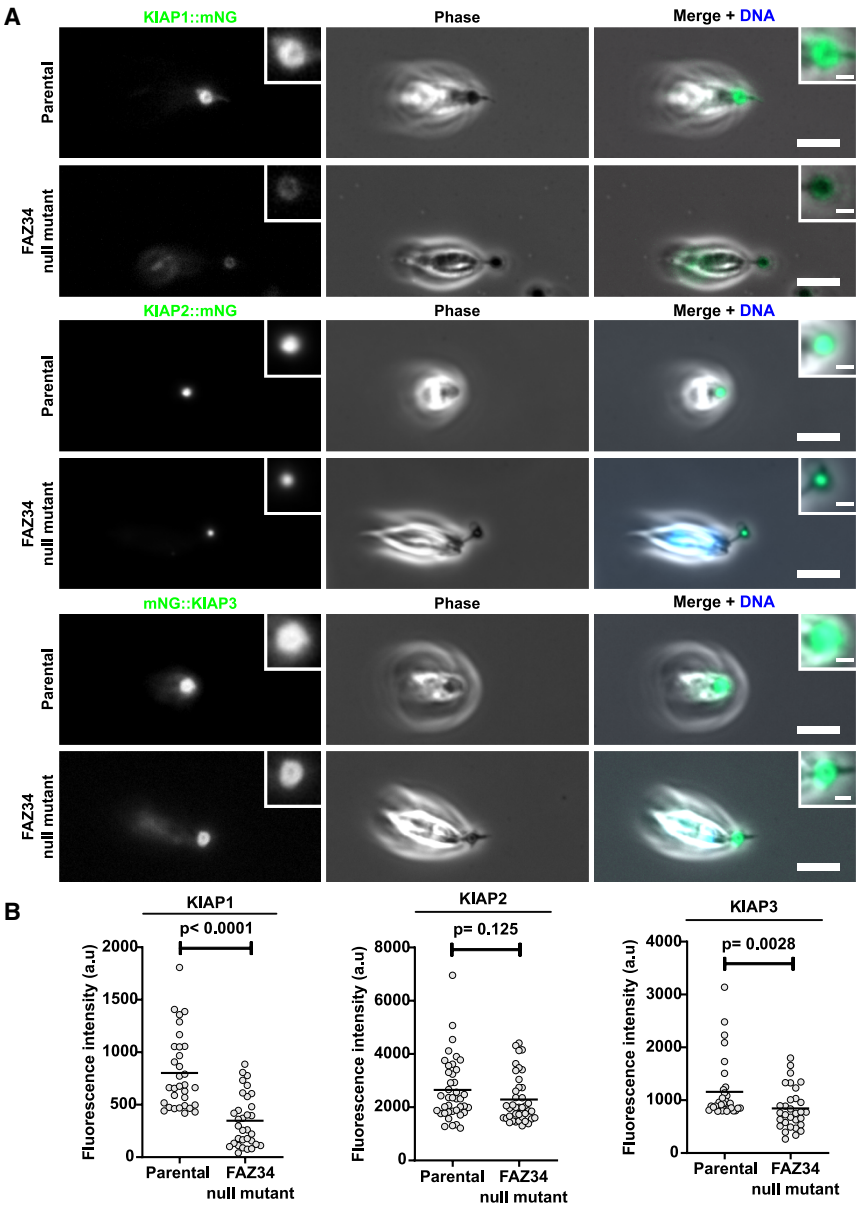

Figure 3. FAZ34 is required for the integration of KIAP1 and KIAP3 into the adhesion plaque

(A) Localization of mNG-tagged KIAP1, KIAP2, and KIAP3 in parental and FAZ34 null mutant *L. mexicana* haptomonad-like cells. Insets illustrate a magnified view of KIAP1, KIAP2, and KIAP3 in the adhered flagellum. DNA was stained with Hoechst 33342 (blue). Scale bars, 5 μm; inset, 1 μm.

(B) Quantification of fluorescence intensities of KIAP1 (n = 32 per cell line), KIAP2 (n = 40 per cell line), and KIAP3 (parental, n = 32; FAZ34 null mutant, n = 31) in the adhered flagellum of the parental and FAZ34 null mutant cells after 72 h of adhesion. For fluorescence quantifications, the average intensity was measured within a defined region around the signal on the projected z stack image. The acquired images were 2.25-μm thick in total. The plots show the individual measurements after background correction, with the horizontal bars representing the mean. p values were calculated using the Mann-Whitney test.

See also Figure S3.

filaments, whereas in the FAZ34 null mutant there was a gap (0.42 ± 0.21 μm; n = 46) separating the filaments from the cell tip, which matched our light microscopy observations (Figure 4A).

Given the striking similarity in KIAP2 localization and the position of these filaments on the flagellum, we investigated KIAP2 localization at the ultrastructural level by immunogold, using a cell line expressing KIAP2 endogenously tagged with mNG and 3 Myc epitopes. As a control, we generated a cell line expressing the PFR protein 2 (PFR2) fused to the same tag. PFR2 is one of the two most abundant proteins in the PFR.[25–27] Expression of 3Myc-mNG-tagged KIAP2 and PFR2 was confirmed by immunofluorescence (Figures S4A and S4B). In our electron micrographs of cytoskeletons from cells expressing KIAP2::3Myc::mNG, most gold particles were associated with the filaments, with few or no particles on the PFR and axoneme (Figure 4E). However, in the cells expressing PFR2::3Myc::mNG, most gold particles were associated with the PFR, with few or none on the filaments (Figures S4C and S4D). This shows that KIAP2 is a component of these filaments. Next, we examined detergent-extracted KIAP2 null mutant cytoskeletons by TEM (Figure 4F). In all cytoskeletons examined (n = 18), we did not observe the filament bundles on the flagellum. This suggests that KIAP2 is an essential component of these filaments on the flagellum.

In negatively stained dividing cells with a short new flagellum, we observed that the filaments were only present on the old flagellum but not on the new flagellum, suggesting that the assembly of the filaments occurs after the assembly of the microtubule axoneme (Figure S4E). To determine the stage of the *Leishmania* cell cycle at which the filaments appeared, we analyzed KIAP2::mNG-tagged promastigote cells by fluorescence light microscopy and classified the cells into different cell-cycle stages based on the kinetoplast (K), nucleus (N), and flagellum (F) number.[28] In 1F1K1N cells, we saw a range of KIAP2 signals, with a brighter signal in cells with a longer flagellum than those with a shorter flagellum (Figures S4F and S4G). Moreover, the KIAP2 signal was weaker in the new flagellum of 1K1N2F cells than in the new flagellum of 2K2N2F cells, which had progressed further through the cell cycle (Figure S4F). Generally, the KIAP2 signal was brighter in the older, longer flagella than in the newer, shorter flagella. This confirms that the filaments are assembled into the flagellum after microtubule assembly, with the KIAP2 amount increasing as the new flagellum elongates.

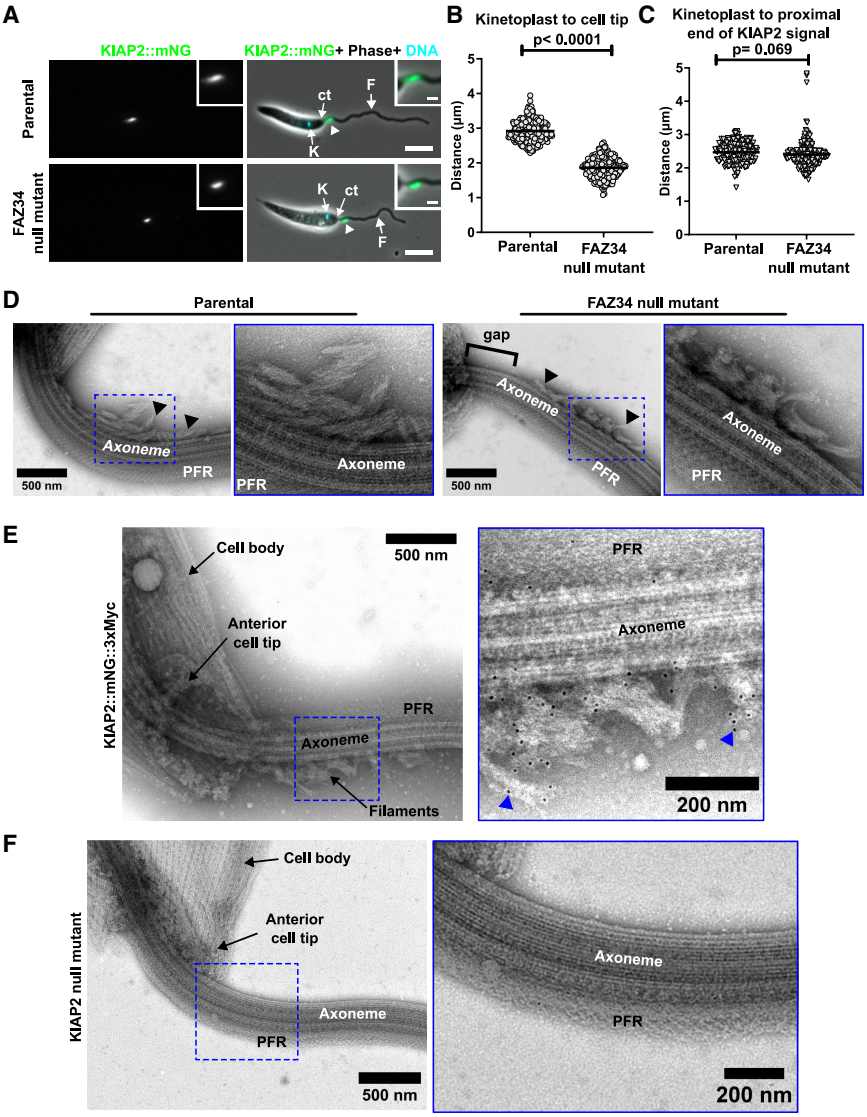

Figure 4. FAZ34 deletion disconnected KIAP2 and a novel set of filaments from the promastigote anterior cell tip

(A) Fluorescence micrographs showing the position of KIAP2 signal (arrowheads) in the parental and FAZ34 null mutant cells. K, kinetoplast; F, flagellum; ct, cell body tip. Scale bars, 5 µm; inset, 1 µm.

(B) Quantification of the distance between the center of the kinetoplast to the anterior cell tip, as a measure of the correct anterior cell tip morphogenesis, in the parental and FAZ34 null mutant cells. Three hundred (n = 300) 1K1N cells were measured for each cell line, and the individual measurements and the mean value (horizontal bar) are shown.

(C) Measurement of the position of KIAP2, defined by the distance between the center of the kinetoplast and the proximal end of KIAP2 signal for the parental and FAZ34 null mutant cells. Data from 200 1K1N cells are plotted, with bar representing the mean. The p values in (B) and (C) were calculated using Welch's t test.

(D) Negatively stained *L. mexicana* parental and FAZ34 null mutant promastigote cell lines showing the ultrastructure of the filaments (arrowheads) as the flagellum emerges from the cell body.

(E) Ultrastructural positioning of KIAP2, by immunogold labeling with 10 nm gold particles. The inset shows a magnified view of the different structures and a high concentration of gold particles (arrowheads) in the filaments. PFR, paraflagellar rod.

(F) Negatively stained KIAP2 null mutant whole-cell cytoskeleton. KIAP2 deletion resulted in the loss of the filaments.

See also Figures S4 and S6.

Deletion of FAZ34 caused cell body mispositioning relative to the adhesion plaque and KIAP2 in adhered haptomonad-like cells

Given the gap seen between both KIAP2 and the filaments and the promastigote anterior cell tip in the FAZ34 null mutant, we revisited our images of adhered cells of the parental and FAZ34 null mutant to determine whether there was a change in haptomonad-like cell morphology. In the *in vitro* promastigote and early stages of haptomonad-like cell differentiation (i and ii), the flagellum appeared thinner as it emerged from the cell body in all the FAZ34 null mutants examined (n = 100 cells) (Figure 5A). This thinner region of the flagellum corresponded to the gap separating the KIAP2 signal and the filaments from the anterior cell tip and was likely caused by the disruption of the anterior cell tip morphology (Figures 4A–4D and S5). In stably adhered FAZ34 null mutants (stages iii–v), there was a gap separating the cell body from the KIAP2 signal and the adhesion plaque (Figures 5A and S5). To characterize the observed phenotype, we acquired z stack images of mature parental and FAZ34 null mutant haptomonad-like cells, after 24 h of adhesion, and compared the distance between the anterior cell body tip and the center of the adhesion plaque. This distance was significantly larger (1.51 ± 0.44 µm; n = 25) in the FAZ34 null mutant compared with the parental cells (0.43 ± 0.07 µm; n = 25) (Figure 5B). However, we did not know whether the increased distance was due to a slower differentiation rate in FAZ34 null mutants. To address this, we allowed the cells to adhere to glass coverslips for 72 h and compared the distances in mature haptomonad-like cells of FAZ34 null mutant and parental cells. The distance between the anterior cell tip and adhesion plaque remained significantly larger (1.37 ± 0.62 µm; n = 70) in the FAZ34 null mutant compared with the parental cells (0.45 ± 0.07 µm; n = 70), and it did not change in comparison to the haptomonad-like cells differentiated for 24 h (Figure 5B). Overall, these findings suggest that correct anterior cell tip morphology, mediated by the presence of FAZ34, is required for the positioning of the cell body adjacent to the adhesion plaque during haptomonad differentiation.

DISCUSSION

Leishmania adhesion to the stomodeal valve of the sand fly occurs via a modified flagellum, which contains an adhesion plaque

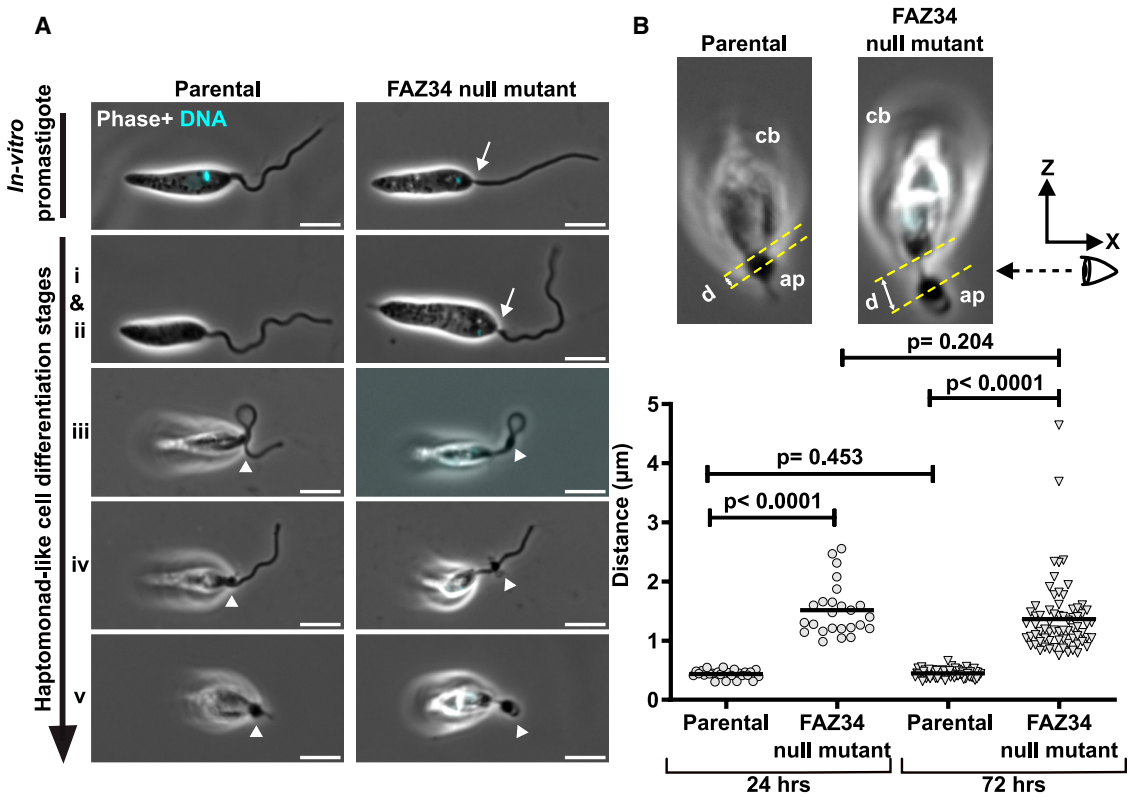

Figure 5. FAZ34 deletion caused cell body mispositioning relative to the adhesion plaque in adhered cells

(A) Phase and Hoechst fluorescence images showing the position of the cell body relative to the adhesion plaque (arrowheads) for the parental and FAZ34 null mutant cells at different haptomonad-like cell differentiation stages (i–v). The arrows show a thinner region of the flagellum as it emerged from the cell body in the FAZ34 null mutant, which was not seen in the parental cells. Scale bars, 5 µm.

(B) Measurement of the distance between the anterior cell body tip and the center of the adhesion plaque for parental and FAZ34 null mutant after 24 and 72 h of haptomonad-like cell differentiation on glass coverslips. For each cell line, 25 and 70 cells were measured after 24 and 72 h of differentiation, respectively. The individual measurements (circles or triangles) and the mean (bar) are shown. The *p* values were calculated using two-tailed Welch's t test.

See also Figure S5.

that interacts with the underlying substrate, plus a filamentous network that extends from the plaque and likely connects to the cell body via the FAZ.[18] Strong adhesion requires the progressive disassembly of the long motile flagellum of the promastigote form into a shorter, highly specialized adhesive flagellum of the haptomonad, with accompanying structural and molecular changes to the anterior cell tip.[18] Here, we show that the FAZ undergoes a molecular rearrangement during haptomonad differentiation, with a reorganization of FAZ proteins from a short, linear structure within the flagellar pocket neck region to a C-shaped structure that faces the adhesion plaque. This rearrangement aligns with our previous serial electron tomography data, which showed a reorganization of the flagellar pocket neck and FAZ region of the cell, which leads to an expansion of the FAZ area facing toward the adhesion plaque.[18] The remodeling of the FAZ and anterior cell tip will also likely rely on a reorganization of the cortical microtubule cytoskeleton in this region. The FAZ reorganization at the anterior cell tip coincided with the enlargement of the flagellum tip, which is associated with the final stages of adhesion plaque assembly and maturation and is likely required to form a strong cytoskeletal connection extending from the cell body to the adhesion plaque.

The FAZ is important for anterior cell tip and flagellar pocket morphogenesis in *Leishmania*, with the loss of FAZ proteins associated with a reduction in the kinetoplast-to-cell-tip distance.[19,20,22] Moreover, FAZ5 deletion resulted in the loss of the distinctive asymmetric cell tip, where the cell body extends further along the side of the flagellum associated with the FAZ,[20] whereas the loss of FAZ2 resulted in an extension of this asymmetry, with the cell body extending further along the flagellum.[19] The FAZ is a complex cytoskeletal structure, with distinct cell body, intermembrane, and flagellum domains. Deletion of proteins from each of these domains (FAZ2, cell body; FAZ5, intermembrane; and FAZ34, flagellum) severely impaired the adhesion ability of *Leishmania* parasites *in vitro*. Moreover, in the FAZ34 null mutant, there were defects in adhesion plaque assembly, with reduced levels of KIAP1 and KIAP3 in the adhesion plaque and a reduced plaque size. These defects likely translate to a weaker connection to the underlying substrate, reflected in the reduced number of stably adhered parasites (model in Figure 6). Overall, this demonstrates the importance of the FAZ for the establishment of strong and stable adhesion to a substrate, with disruption of anterior cell tip morphogenesis likely causing defects in adhesion plaque assembly.

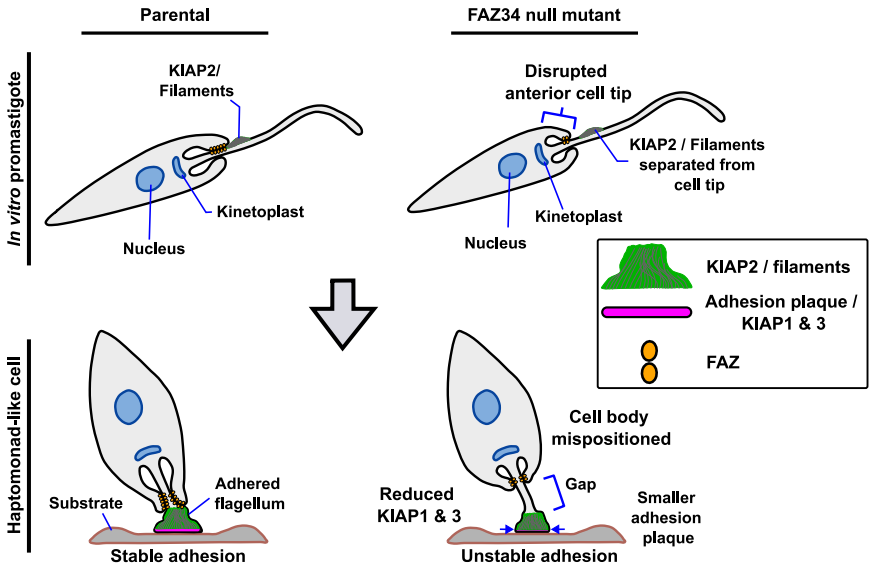

Figure 6. Model of the roles of FAZ in *Leishmania* adhesion

A schematic of the parental and FAZ34 null mutant promastigote and haptomonad-like cells based on *in vitro* observations. FAZ34 deletion disrupts the anterior cell tip morphology, resulting in the separation of KIAP2 and the flagellar filaments from the anterior cell tip in the promastigote and haptomonad-like cells, with the cell tip positioned further from the adhesion plaque in the latter when compared with parental cells. This is associated with defects in adhesion plaque assembly, with lower levels of KIAP1 and KIAP3 in the plaque and a reduced plaque size, which translates to unstable adhesion in the FAZ34 null mutant.
See also Figure S6.

The localization of KIAP2 to a region of the flagellum in promastigotes, as it emerges from the cell body, prompted us to investigate the ultrastructure of this region. We identified a novel set of filament bundles in this much-studied stage of the life cycle that lay parallel to the axoneme, on the opposite side to the PFR and adjacent to the anterior cell tip. KIAP2 localization to these filaments was confirmed by immunogold staining and its presence was required for their assembly. KIAP2 encodes a calpain-like protease domain that lacks the catalytic residues, and this domain is thought to mediate protein-protein interactions. It is likely that KIAP2 is the main component of these novel filaments; however, its filament-forming capabilities have yet to be investigated. Alternatively, KIAP2 may be important for stabilizing filaments formed by an additional, as-yet-unidentified protein. We have shown that, in the modified flagellum of haptomonads, there is a filamentous network extending from the adhesion plaque to the cell body, with KIAP2 potentially localized along these filaments.[15,18] The presence of KIAP2-containing filaments in the proximal region of the promastigote flagellum and the modified haptomonad flagellum indicates that these filaments will likely have common constituents. Given that KIAP2 is required for both parasite adhesion[15] and filament formation, this suggests that these filaments are also central to *Leishmania* adhesion.

In *Leishmania*, the initial site of adhesion can occur at any point along the flagellum, and during subsequent haptomonad maturation, the cell body moves toward the adhesion site.[15] In adhering cells in which adhesion initiates at a distance from the cell body, KIAP2 is found in two foci: one corresponding to the adhesion site and the other the region of the flagellum adjacent to the anterior cell tip, with a weaker KIAP2 signal connecting these two foci.[15] This KIAP2 localization pattern suggests that the KIAP2-containing filaments may play a role in the movement of the cell body to the adhesion plaque. In dividing cells, we saw that the KIAP2 signal was initially absent in the new flagellum, with longer flagella having a brighter signal. This shows that these filaments are assembled into the flagellum after microtubule axoneme assembly, similar to the PFR.[26,29] Moreover, the post-axonemal assembly of KIAP2 will likely impact the adhesive capacity of the daughter cell that inherits the new flagellum. One might envisage that a cell inheriting the new flagellum, with less KIAP2, will be less likely to adhere at the start of the cell cycle than later when the amount of KIAP2 in the flagellum has increased.

In the FAZ34 null mutant promastigotes, the close association between the KIAP2, flagellar filaments, and the anterior cell tip was lost, resulting in a separation between the KIAP2, flagellar filaments, and anterior cell tip (Figure 6). This separation was also seen in the adhered FAZ34 null mutants, with the cell tip positioned further from the adhesion plaque when compared with parental cells. The separation between the cell tip and the adhesion plaque observed in the adhered FAZ34 null mutant is likely due to the disruption of the anterior cell tip morphology caused by the loss of FAZ34.[22] This suggests that the close association of KIAP2 and the flagellar filaments with the anterior cell tip is required for stable parasite adhesion and is mediated by the FAZ.

Intriguingly, in the FAZ34 null mutant, the distance from the kinetoplast to the KIAP2 signal remained constant, whereas the distance from the kinetoplast to the anterior cell tip dropped. This suggests that the KIAP2 position is determined by a flagellum-based mechanism that is not dependent on any feedback from the cell body. A similar phenomenon has been described for the positioning of the PFR in *Trypanosoma brucei*.[30] Although the details of this mechanism have yet to be determined, it may be due to specific marks on axoneme acting as an internal ruler and/or related to proximal/distal asymmetries observed in the *Leishmania* flagellum, with a change in the proteins associated with the outer microtubule doublets occurring around this point in the flagellum.[31,32] These flagellar filaments have not been explicitly described in *Leishmania* before; however, when we revisited our collection of thin-section transmission electron micrographs of this region of the cell, we often saw a bulge in the flagellum as it emerged from the cell body (Figures S6A and S6B). In this bulge, there was little pattern to the electron density, so we suspect that these filaments are not well preserved and/or stained using traditional EM fixatives and methodologies. A contributing factor to the difficulty in discerning these filaments may be their packing state, with the filaments tightly packed in a whole cell, whereas in

detergent-treated cells, the filaments may "relax," enabling better staining. The bulge is also found on the side of the flagellum associated with the FAZ (Figures S6A and S6B), further supporting the potential connections between these flagellar filaments and the FAZ. Interestingly, filaments have been observed in the flagellum of *Crithidia fasciculata* in a similar position and *Paratrypanosoma confusum* has a large bulge in its flagellum as it emerges from the cell body.[33–35] In the latter case, this large bulge is associated with the adhesion of this parasite to a substrate.[33] This suggests that these flagellar filaments are an ancestral feature of the kinetoplastid parasites that adopt a liberform morphology[36] and are likely important for their adhesion to a range of substrates. Yet KIAP2 is widely conserved across the kinetoplastids found in both liberform and juxtaform parasites (Figure S6C). In the TrypTag localization project, KIAP2 was found in the cytoplasm and flagellum of the *T. brucei* insect form, so it will be of interest to determine the specific structure that KIAP2 localizes to in this species. Finally, the presence of these filaments in the flagellum of motile stages indicates that *Leishmania* parasites are primed for adhesion, with molecular components already present, enabling the efficient establishment of a stable connection to a substrate.

In conclusion, we have identified and initially characterized a new set of flagellar filaments that contain the adhesion protein KIAP2 and likely act as a coordinating foundational structure for parasite adhesion, while also showing the importance of maintaining a connection from adhesion plaque through to the cell body for stable *Leishmania* adhesion to a substrate.

RESOURCE AVAILABILITY

Lead contact

Requests for further information, resources, and reagents should be directed to, and will be fulfilled by, the lead contact, Jack Sunter (jsunter@brookes.ac.uk).

Materials availability

All unique/stable reagents generated in this study are available from the lead contact with a completed materials transfer agreement.

Data and code availability

- All data reported in this paper will be shared by the lead contact upon request.
- This study did not generate any unique code.
- Any additional information required to reanalyze the data reported in this paper is available from the lead contact upon request.

ACKNOWLEDGMENTS

B.O.O. was funded by the Nigel Groome PhD studentship, and work in the Sunter lab is supported by the Wellcome Trust (221944/Z/20/Z). We thank Dr. Clare Halliday (Oxford Brookes University) and Ed Rea (Oxford Brookes University) for providing electron micrographs and Dr. Jorge Arias Del Angel (University of Würzburg) for assistance with developing scripts for area measurements. We thank Dr. Richard Wheeler (University of Edinburgh), Dr. Uli Dobramysl (University of Oxford), and Prof. Keith Gull (University of Oxford) for many discussions. We also acknowledge the expertise of the Oxford Brookes University Centre for Bioimaging.

AUTHOR CONTRIBUTIONS

B.O.O. performed experiments, developed methodology and analysis, and contributed to writing. R.Y. performed experiments and contributed to supervision and writing. A.O.M. and F.M.-L. performed experiments, developed methodology, and contributed to analysis and editing of the manuscript. S. V. contributed to project administration, supervision, and editing of the manuscript. J.D.S. conceptualized the study, analyzed the data, acquired funding, and wrote the manuscript.

DECLARATION OF INTERESTS

The authors declare no competing interests.

STAR★METHODS

Detailed methods are provided in the online version of this paper and include the following:

- KEY RESOURCES TABLE
- EXPERIMENTAL MODEL AND STUDY PARTICIPANT DETAILS
  - Cell culture
- METHOD DETAILS
  - Tagging, deletion and add-back generation
  - Growth curves
  - Haptomonad-like cells differentiation assays
  - *In vitro* haptomonad-like cells adhesion quantification
  - Widefield microscopy
  - Confocal microscopy
  - Immunofluorescence microscopy
  - Negative staining
  - Immunogold labelling
  - Bioinformatics analyses
- QUANTIFICATION AND STATISTICAL ANALYSIS
  - Statistical analysis

SUPPLEMENTAL INFORMATION

Supplemental information can be found online at https://doi.org/10.1016/j.cub.2025.04.064.

Received: February 27, 2025
Revised: April 22, 2025
Accepted: April 25, 2025
Published: May 20, 2025

REFERENCES

1. Darby, C. (2008). Uniquely insidious: *Yersinia pestis* biofilms. Trends Microbiol. *16*, 158–164. https://doi.org/10.1016/j.tim.2008.01.005.
2. WHO (2023). Leishmaniasis. https://www.who.int/news-room/fact-sheets/detail/leishmaniasis.
3. CDC (2020). Leishmaniasis. https://www.cdc.gov/parasites/leishmaniasis/gen_info/faqs.html.
4. Bailey, F., Mondragon-Shem, K., Hotez, P., Ruiz-Postigo, J.A., Al-Salem, W., Acosta-Serrano, Á., and Molyneux, D.H. (2017). A new perspective on cutaneous leishmaniasis—Implications for global prevalence and burden of disease estimates. PLoS Negl. Trop. Dis. *11*, e0005739. https://doi.org/10.1371/journal.pntd.0005739.
5. Owino, B.O., Matoke-Muhia, D., Alraey, Y., Mwangi, J.M., Ingonga, J.M., Ngumbi, P.M., Casas-Sanchez, A., Acosta-Serrano, A., and Masiga, D.K. (2019). Association of *Phlebotomus guggisbergi* with *Leishmania major* and *Leishmania tropica* in a complex transmission setting for cutaneous leishmaniasis in Gilgil, Nakuru County, Kenya. PLoS Negl. Trop. Dis. *13*, e0007712. https://doi.org/10.1371/journal.pntd.0007712.
6. Ghosh, S., Verma, A., Kumar, V., Pradhan, D., Selvapandiyan, A., Salotra, P., and Singh, R. (2020). Genomic and transcriptomic analysis for identification of genes and interlinked pathways mediating artemisinin resistance in *Leishmania donovani*. Genes (Basel) *11*, 1362. https://doi.org/10.3390/genes11111362.

7. Serafim, T.D., Coutinho-Abreu, I.V., Dey, R., Kissinger, R., Valenzuela, J. G., Oliveira, F., and Kamhawi, S. (2021). Leishmaniasis: the act of transmission. Trends Parasitol. *37*, 976–987. https://doi.org/10.1016/j.pt.2021.07.003.

8. Sunter, J., and Gull, K. (2017). Shape, form, function and *Leishmania* pathogenicity: From textbook descriptions to biological understanding. Open Biol. *7*, 170165. https://doi.org/10.1098/rsob.170165.

9. Dostálová, A., and Volf, P. (2012). *Leishmania* development in sand flies: Parasite-vector interactions overview. Parasites Vectors *5*, 1.

10. Gossage, S.M., Rogers, M.E., and Bates, P.A. (2003). Two separate growth phases during the development of *Leishmania* in sand flies: Implications for understanding the life cycle. Int. J. Parasitol. *33*, 1027–1034. https://doi.org/10.1016/s0020-7519(03)00142-5.

11. Coutinho-Abreu, I.V., Serafim, T.D., Meneses, C., Kamhawi, S., Oliveira, F., and Valenzuela, J.G. (2020). Distinct gene expression patterns in vector-residing *Leishmania infantum* identify parasite stage-enriched markers. PLoS Negl. Trop. Dis. *14*, e0008014. https://doi.org/10.1371/journal.pntd.0008014.

12. Rogers, M.E., Chance, M.L., and Bates, P.A. (2002). The role of promastigote secretory gel in the origin and transmission of the infective stage of the infective stage of *Leishmania mexicana* by the sandfly *Lutzomyia longipalpis*. Parasitology *124*, 495–507. https://doi.org/10.1017/s0031182002001439.

13. Rogers, M.E., and Bates, P.A. (2007). *Leishmania* manipulation of sand fly feeding behavior results in enhanced transmission. PLoS Pathog. *3*, e91. https://doi.org/10.1371/journal.ppat.0030091.

14. Catta-Preta, C.M.C., Ghosh, K., Sacks, D.L., and Ferreira, T.R. (2024). Single- cell atlas of *Leishmania* development in sandflies reveals the heterogeneity of transmitted parasites and their role in infection. Proc. Natl. Acad. Sci. USA *121*, e2406776121. https://doi.org/10.1073/pnas.2406776121.

15. Yanase, R., Pružinová, K., Owino, B.O., Rea, E., Moreira-Leite, F., Taniguchi, A., Nonaka, S., Sádlová, J., Vojtkova, B., Volf, P., and Sunter, J.D. (2024). Discovery of essential kinetoplastid-insect adhesion proteins and their function in *Leishmania*-sand fly interactions. Nat. Commun. *15*, 6960.

16. Rogers, M.E., Hajmová, M., Joshi, M.B., Sadlova, J., Dwyer, D.M., Volf, P., and Bates, P.A. (2008). *Leishmania* chitinase facilitates colonization of sand fly vectors and enhances transmission to mice. Cell. Microbiol. *10*, 1363–1372. https://doi.org/10.1111/j.1462-5822.2008.01132.x.

17. Bates, P.A. (2007). Transmission of *Leishmania* metacyclic promastigotes by phlebotomine sand flies. Int. J. Parasitol. *37*, 1097–1106. https://doi.org/10.1016/j.ijpara.2007.04.003.

18. Yanase, R., Moreira-Leite, F., Rea, E., Wilburn, L., Sádlová, J., Vojtkova, B., Pružinová, K., Taniguchi, A., Nonaka, S., Volf, P., et al. (2023). Formation and three-dimensional architecture of *Leishmania* adhesion in the sand fly vector. eLife *12*, e84552. https://doi.org/10.7554/eLife.84552.

19. Halliday, C., Yanase, R., Catta-Preta, C.M.C., Moreira-Leite, F., Myskova, J., Pruzinova, K., Volf, P., Mottram, J.C., and Sunter, J.D. (2020). Role for the flagellum attachment zone in *Leishmania* anterior cell tip morphogenesis. PLoS Pathog. *16*, e1008494. https://doi.org/10.1371/journal.ppat.1008494.

20. Sunter, J.D., Yanase, R., Wang, Z., Catta-Preta, C.M.C., Moreira-Leite, F., Myskova, J., Pruzinova, K., Volf, P., Mottram, J.C., and Gull, K. (2019). *Leishmania* flagellum attachment zone is critical for flagellar pocket shape, development in the sand fly, and pathogenicity in the host. Proc. Natl. Acad. Sci. USA *116*, 6351–6360. https://doi.org/10.1073/pnas.1812462116.

21. Wheeler, R.J., Sunter, J.D., and Gull, K. (2016). Flagellar pocket restructuring through the *Leishmania* life cycle involves a discrete flagellum attachment zone. J. Cell Sci. *129*, 854–867. https://doi.org/10.1242/jcs.183152.

22. Halliday, C., de Liz, L.V., Vaughan, S., and Sunter, J.D. (2023). Disruption of *Leishmania* flagellum attachment zone architecture causes flagellum loss. Mol. Microbiol. 1–16.

23. Corrales, R.M., Vaselek, S., Neish, R., Berry, L., Brunet, C.D., Crobu, L., Kuk, N., Mateos-Langerak, J., Robinson, D.R., Volf, P., et al. (2021). The kinesin of the flagellum attachment zone in Leishmania is required for cell morphogenesis, cell division and virulence in the mammalian host. PLoS Pathog. *17*, 1–29.

24. Molyneux, D.H., Wallbanks, K.R., and Ingram, G.A. (1987). Trypanosomatid-Vector Interfaces- In Vitro Studies on Parasite Substrate Interactions, Eleventh Edition (Springer Berlin Heidelberg). https://doi.org/10.1007/978-3-642-72840-2.

25. Santrich, C., Moore, L., Sherwin, T., Bastin, P., Brokaw, C., Gull, K., and Lebowitz, J.H. (1997). A motility function for the paraflagellar rod of *Leishmania* parasites revealed by PFR-2 gene knockouts. Mol. Biochem. Parasitol. *90*, 95–109. https://doi.org/10.1016/s0166-6851(97)00149-7.

26. Bastin, P., MacRae, T.H., Francis, S.B., Matthews, K.R., and Gull, K. (1999). Flagellar morphogenesis: protein targeting and assembly in the paraflagellar rod of trypanosomes. Mol. Cell. Biol. *19*, 8191–8200. https://doi.org/10.1128/MCB.19.12.8191.

27. Portman, N., and Gull, K. (2010). The paraflagellar rod of kinetoplastid parasites: From structure to components and function. Int. J. Parasitol. *40*, 135–148. https://doi.org/10.1016/j.ijpara.2009.10.005.

28. Wheeler, R.J., Gluenz, E., and Gull, K. (2011). The cell cycle of *Leishmania*: Morphogenetic events and their implications for parasite biology. Mol. Microbiol. *79*, 647–662. https://doi.org/10.1111/j.1365-2958.2010.07479.x.

29. Alves, A.A., Gabriel, H.B., Bezerra, M.J.R., de Souza, W., Vaughan, S., Cunha-e-Silva, N.L., and Sunter, J.D. (2020). Control of assembly of extra-axonemal structures: The paraflagellar rod of trypanosomes. J. Cell Sci. *133*, jcs242271. https://doi.org/10.1242/jcs.242271.

30. Bonhivers, M., Nowacki, S., Landrein, N., and Robinson, D.R. (2008). Biogenesis of the trypanosome endo-exocytotic organelle is cytoskeleton mediated. PLoS Biol. *6*, e105. https://doi.org/10.1371/journal.pbio.0060105.

31. Edwards, B.F.L., Wheeler, R.J., Barker, A.R., Moreira-Leite, F.F., Gull, K., and Sunter, J.D. (2018). Direction of flagellum beat propagation is controlled by proximal/distal outer dynein arm asymmetry. Proc. Natl. Acad. Sci. USA *115*, E7341–E7350. https://doi.org/10.1073/pnas.1805827115.

32. Subota, I., Julkowska, D., Vincensini, L., Reeg, N., Buisson, J., Blisnick, T., Huet, D., Perrot, S., Santi-Rocca, J., Duchateau, M., et al. (2014). Proteomic analysis of intact flagella of procyclic *Trypanosoma brucei* cells identifies novel flagellar proteins with unique sub-localization and dynamics. Mol. Cell. Proteomics *13*, 1769–1786. https://doi.org/10.1074/mcp.M113.033357.

33. Skalický, T., Dobáková, E., Wheeler, R.J., Tesařová, M., Flegontov, P., Jirsová, D., Votýpka, J., Yurchenko, V., Ayala, F.J., and Lukeš, J. (2017). Extensive flagellar remodeling during the complex life cycle of *Paratrypanosoma*, an early-branching trypanosomatid. Proc. Natl. Acad. Sci. USA *114*, 11757–11762. https://doi.org/10.1073/pnas.1712311114.

34. Brooker, B.E. (1971). The fine structure of *Crithidia fasciculata* with special reference to the organelles involved in the ingestion and digestion of protein. Z. Zellforsch. Mikrosk. Anat. *116*, 532–563. https://doi.org/10.1007/BF00335057.

35. Denecke, S., Malfara, M.F., Hodges, K.R., Holmes, N.A., Williams, A.R., Julia, H., Pascarella, J.M., Daniels, A.M., Sterk, G.J., Leurs, R., et al. (2024). Adhesion of *Crithidia fasciculata* promotes a rapid change in developmental fate driven by cAMP signaling. mSphere *9*, 1. https://doi.org/10.1128/msphere.00617-24.

36. Wheeler, R.J., Gluenz, E., and Gull, K. (2013). The limits on trypanosomatid morphological diversity. PLoS One *8*, e79581. https://doi.org/10.1371/journal.pone.0079581.

37. Beneke, T., Demay, F., Hookway, E., Ashman, N., Jeffery, H., Smith, J., Valli, J., Becvar, T., Myskova, J., Lestinova, T., et al. (2019). Genetic dissection of a Leishmania flagellar proteome demonstrates requirement

for directional motility in sand fly infections. PLoS Pathog. *15*, e1007828. https://doi.org/10.1371/journal.ppat.1007828.

38. Halliday, C. (2021) The role of the flagellum attachment zone in *Leishmania mexicana* flagellar pocket architecture. PhD thesis (Oxford Brookes University). http://doi.org/10.24384/14dq-ae80.

39. Beneke, T., Madden, R., Makin, L., Valli, J., Sunter, J., and Gluenz, E. (2017). A CRISPR Cas9 high-throughput genome editing toolkit for kinetoplastids. R. Soc. Open Sci. *4*, 170095. https://doi.org/10.1098/rsos.170095.

40. Schindelin, J., Arganda-Carrera, I., Frise, E., Verena, K., Mark, L., Tobias, P., Stephan, P., Curtis, R., Stephan, S., Benjamin, S., et al. (2009). Fiji – an Open platform for biological image analysis. Nat. Methods *9*, 1–15. https://doi.org/10.1038/nmeth.2019.Fiji.

41. Dean, S., Sunter, J., Wheeler, R.J., Hodkinson, I., Gluenz, E., and Gull, K. (2015). A toolkit enabling efficient, scalable and reproducible gene tagging in trypanosomatids. Open Biol. *5*, 140197. https://doi.org/10.1098/rsob.140197.

42. Mazo, G. (2021). QuickFigures: A toolkit and ImageJ PlugIn to quickly transform microscope images into scientific figures. PLoS One *16*, e0240280. https://doi.org/10.1371/journal.pone.0240280.

43. Dean, S., and Sunter, J. (2020). Light microscopy in trypanosomes: use of fluorescent proteins and tags. Methods Mol. Biol. *2116*, 367–383. https://doi.org/10.1007/978-1-0716-0294-2_23.

44. Biomatters (2025). Geneious Prime Version 2025.1. https://www.geneious.com.

45. Katoh, K., and Standley, D.M. (2013). MAFFT multiple sequence alignment software version 7: Improvements in performance and usability. Mol. Biol. Evol. *30*, 772–780. https://doi.org/10.1093/molbev/mst010.

46. Katoh, K., Misawa, K., Kuma, K.I., and Miyata, T. (2002). MAFFT: A novel method for rapid multiple sequence alignment based on fast Fourier transform. Nucleic Acids Res. *30*, 3059–3066. https://doi.org/10.1093/nar/gkf436.

47. Guindon, S., Dufayard, J.F., Lefort, V., Anisimova, M., Hordijk, W., and Gascuel, O. (2010). New algorithms and methods to estimate maximum-likelihood phylogenies: Assessing the performance of PhyML 3.0. Syst. Biol. *59*, 307–321. https://doi.org/10.1093/sysbio/syq010.

48. Stamatakis, A. (2014). RAxML version 8: A tool for phylogenetic analysis and post-analysis of large phylogenies. Bioinformatics *30*, 1312–1313. https://doi.org/10.1093/bioinformatics/btu033.

49. Altschul, S.F., Gish, W., Miller, W., Myers, E.W., and Lipman, D.J. (1990). Basic local alignment search tool. J. Mol. Biol. *215*, 403–410. https://doi.org/10.1016/S0022-2836(05)80360-2.

STAR★METHODS

KEY RESOURCES TABLE

REAGENT or RESOURCE	SOURCE	IDENTIFIER
Antibodies		
c-Myc Monoclonal Antibody (9E10)	Thermofisher	Catalog # MA1-980; RRID: AB_558470
Goat anti-mouse Alexa Fluor 546	Thermofisher	Catalog # A-11030; RRID: AB_2737024
Goat anti-mouse IgG gold	Sigma-Aldrich	Catalog # G7652; RRID: AB_259958
Bacterial and virus strains		
SURE 2 Supercompetent Cells	Agilent Technologies	Catalog # 200152
Chemicals, peptides, and recombinant proteins		
Hoechst 33342	Sigma-Aldrich	Catalog # B2261-25MG
Paraformaldehyde 16%	Thermofisher	Catalog # 043368.9L; 043368.9M
IGEPAL CA-630	Sigma-Aldrich	Catalog # I3021
Glutaraldehyde 25% EM -250ML	TAAB Laboratories Equipment Ltd	Catalog # G003
Experimental models: Cell lines		
L. mexicana MNYC/BZ/1962/M379 Cas9T7	Beneke et al.[37]	N/A
L. mexicana MNYC/BZ/1962/M379 Cas9T7 FAZ5::mNG_FAZ2::mCh	Halliday et al.[22,38]	N/A
L. mexicana MNYC/BZ/1962/M379 Cas9T7 mNG::FAZ34_FLA1BP::mCh	Halliday et al.[22,38]	N/A
L. mexicana MNYC/BZ/1962/M379 SMP1::eGFP	Sunter et al.[20]	N/A
L. mexicana MNYC/BZ/1962/M379 SMP1::eGFP_FAZ2KO	Halliday et al.[19]	N/A
L. mexicana MNYC/BZ/1962/M379 SMP1::eGFP_ FAZ2KO_FAZ2::mCh add-back	Halliday et al.[19]	N/A
L. mexicana MNYC/BZ/1962/M379 SMP1::eGFP_FAZ5KO	Sunter et al.[20]	N/A
L. mexicana MNYC/BZ/1962/M379 SMP1::eGFP_ FAZ5KO_FAZ5::mCh add-back	Sunter et al.[20]	N/A
L. mexicana MNYC/BZ/1962/M379 SMP1::eGFP _FAZ5KO_FAZ5 add-back	This paper	N/A
L. mexicana MNYC/BZ/1962/M379 Cas9T7 FAZ34KO	Halliday et al.[22,38]	N/A
L. mexicana MNYC/BZ/1962/M379 Cas9T7 FAZ34KO_mNG::FAZ34 add-back	Halliday et al.[22,38]	N/A
L. mexicana MNYC/BZ/1962/M379 Cas9T7 KIAP1::mNG	This paper	N/A
L. mexicana MNYC/BZ/1962/M379 Cas9T7 KIAP1::mNG_FAZ34KO	This paper	N/A
L. mexicana MNYC/BZ/1962/M379 Cas9T7 KIAP2::mNG	This paper	N/A
L. mexicana MNYC/BZ/1962/M379 Cas9T7 KIAP2::mNG_FAZ34KO	This paper	N/A
L. mexicana MNYC/BZ/1962/M379 Cas9T7 mNG::KIAP3	This paper	N/A
L. mexicana MNYC/BZ/1962/M379 Cas9T7 mNG::KIAP3_FAZ34KO	This paper	N/A
L. mexicana MNYC/BZ/1962/M379 Cas9T7 KIAP2KO	Yanase et al.[15]	N/A
L. mexicana MNYC/BZ/1962/M379 Cas9T7 FAZ10::mNG_FLA1BP::mCh	Halliday et al.[22,38]	N/A
L. mexicana MNYC/BZ/1962/M379 Cas9T7 mNG::FAZ34_KIAP1::mCh	This paper	N/A
L. mexicana MNYC/BZ/1962/M379 Cas9T7 mNG::FAZ34_KIAP2::mCh	This paper	N/A
L. mexicana MNYC/BZ/1962/M379 Cas9T7 mNG::FAZ34_ mCh::KIAP3	This paper	N/A
L. mexicana MNYC/BZ/1962/M379 Cas9T7 SMP1::mCh	This paper	N/A
L. mexicana MNYC/BZ/1962/M379 Cas9T7 SMP1::mCh_FAZ34KO	This paper	N/A
L. mexicana MNYC/BZ/1962/M379 Cas9T7 mNG::PFR2	This paper	N/A
Oligonucleotides		
FAZ5 gene deletion and add-back confirmation primers: Forward: atatataagcttATGTGCAACGGCCACCCGCC; Reverse: atatatagatctCTACCTCTTCCTCTCCGCGCC	This paper	N/A

(*Continued on next page*)

Continued

REAGENT or RESOURCE	SOURCE	IDENTIFIER
500 bp FAZ34 ORF internal control primers: Forward: CGTAGGCGTGTTCAAGAATC; Reverse: ACACTTGCGGGTACTTCTG	This paper	N/A
Tagging and gene deletion primers and sgRNAs were designed using LeishGEdit (http://www.leishGEdit.net)	Beneke et al.[39]	N/A
Recombinant DNA		
pPLOTv1	Beneke et al.[39]	N/A
pLPOT	Edwards et al.[31]	N/A
pTBlast_v1	Beneke et al.[39]	N/A
pTNeo_v1	Beneke et al.[39]	N/A
pTPuro_v1	Beneke et al.[39]	N/A
Software and algorithms		
Fiji	Schindelin et al.[40]	https://imagej.net/software/fiji
MATLAB (R2023a)	MathWorks	https://uk.mathworks.com/products/new_products/release2023a.html
Geneious prime (v2025.1)	Biomatters	https://www.geneious.com
GraphPad Prism (v9.5)	GraphPad	https://www.graphpad.com

EXPERIMENTAL MODEL AND STUDY PARTICIPANT DETAILS

Cell culture

Leishmania mexicana promastigotes (WHO strain MNYC/BZ/62/M379), expressing Cas9 nuclease and T7 polymerase were grown at 28°C in M199 medium with Earle's salts and L-glutamine (Life Technologies), 26 mM $NaHCO_3$, 5 μg/mL haemin, 40 mM HEPES-HCL (pH 7.4) and 10% fetal bovine serum (FBS). The cells were maintained in the logarithmic growth phase by regular sub culturing.

METHOD DETAILS

Tagging, deletion and add-back generation

Constructs and single guide RNAs (sgRNAs) for endogenous mNeonGreen or mCherry tagging of *L. mexicana* FAZ, PFR2, SMP1 and KIAPs 1-3 genes were generated by PCR method, according to Dean et al.[41] and Beneke et al.,[39] using pPLOT plasmids with either blasticidin, puromycin or neomycin resistance genes as the templates, or pLPOT plasmid with blasticidin resistance gene as the template.[31] The FAZ gene deletion constructs were generated by PCR using two pT plasmids with different resistance genes (blasticidin, puromycin or neomycin) and the G00 as the template.[39] Primers and sgRNAs for the tagging and deletion constructs were designed using LeishGEdit (http://www.leishGEdit.net).[39] FAZ5 add-back construct was generated as previously described.[20,38] The FAZ5 (*LmxM.36.5970*) open reading frame was amplified by PCR using manually designed primers containing *HindIII* and *BglII* restriction sites. The PCR products were digested with either *HindIII* and *BglII* and ligated into pJ1252 plasmid at the *HindIII* and *BamHI* restriction sites, then transformed into 20 μl of *E. coli* SURE 2 Supercompetent cells (Agilent Technologies; 200152) using the heat shock method at 42 °C for 50 seconds. 10 μg of the recovered plasmid construct was linearised using *PacI* and precipitated with 3 M sodium acetate (pH 5.2) and 100% ethanol. The pellet was washed with 70% ethanol and resuspended in 20 μl sterile molecular grade H_2O before transfection. All the transfections were performed using the X-001 programme on the Amaxa Nucleofector II device and successful transfectants selected, after 6 hours, using blasticidin (5 μg/ml), puromycin (20 μg/ml) or G-418 (20 μg/ml) (Melford Laboratories).

Growth curves

Leishmania mexicana promastigotes were set up at 1 x 10^5 cells/ mL in M199 supplemented with 10% FBS. Cumulative cell growth was measured daily by counting the number of cells using the Beckman Coulter Counter.

Haptomonad-like cells differentiation assays

Axenic haptomonad cells were generated according to Yanase et al.[18] Briefly, gridded glass coverslips grid-500, (ibidi; 10816) were cut into ~5 x 5 mm pieces and sterilized with 100% ethanol for 5 min in a sterile Petri dish. The coverslips were washed twice with 5 ml of M199 media, transferred to a 24-well plate containing 1 mL of M199 medium, and washed two more times with 1 mL of M199. Following the final wash, promastigotes at 5x10^6 cells/mL of M199 medium were added to the coverslips and allowed to differentiate for 24 h at 28 °C with 5% CO_2.

In vitro haptomonad-like cells adhesion quantification

Gridded glass coverslips grid-500 (ibidi; 10816) were prepared as described above and three coverslips were used for each cell line. Log phase promastigotes of FAZ2, FAZ5 and FAZ34 parental, deletion mutants, and add-back cell lines (5x10^6 cells/mL) were grown on the ~5 x 5 mm pieces in a 24-well plate with 1 mL of M199 medium for 24 h at 28 °C with 5% CO_2. The coverslips were washed twice by transferring them to wells with 1 mL DMEM, and then incubated with 1 mL DMEM containing 1 μg/mL of Hoechst 33342 for 5 min. The coverslips were then washed twice with 1 mL DMEM and mounted, with the top side facing up, on a super frost microscope slide with premarked circular wells, created using the ImmEdge hydrophobic barrier pen (Vector laboratories; H-4000). Another glass coverslip was mounted carefully onto the gridded coverslips to avoid air bubbles. Adhered cells were imaged in a 500 μm x 500 μm grid area using the Zeiss Axio ImagerZ2 upright microscope with the Zeiss Plan-Apochromat 20x/0.8NA PH2 objective and Hamamatsu Flash 4 camera (Hamamatsu Photonics, Hamamatsu, Japan). Images of adhered cells in five different grids were acquired for each coverslip using the phase (5 ms exposure, TL-VIS LED Lamp illumination) and H3342 (Zeiss filter set 49; 50 ms exposure time, Zeiss HBO100 mercury bulb illumination using Osram HBO103/W2 bulbs) channels in ZEN 2.3 Blue (release version 69.1) software. Adhered cells in each grid area were manually counted in Fiji,[40] using the phase contrast image and Hoechst signal.

Widefield microscopy

For live cell imaging of tagged or untagged *L. mexicana* promastigotes, 1 mL of log phase cell cultures (~1x10^7 cells/mL) were washed twice with 1 mL of DMEM. The cells were resuspended in 1 mL DMEM containing 1 μg/mL of Hoechst 33342 and incubated at RT for 5 min. Following incubation, cells were washed twice with 1 mL of DMEM and resuspended in a 100 μL final volume. One microliter (1 μL) of the cell suspension was added to the centre of premarked circular wells on a super frost microscope slide. The cells were mounted with a glass coverslip and imaged using the Zeiss Axio ImagerZ2 upright microscope with the Zeiss 63x/1.4NA PH3 oil-immersion Plan-Apochromat objective and Hamamatsu Flash 4 camera. For KIAP2 signal intensity observation in dividing cells, we imaged the cells using the Zeiss alpha Plan-Apochromat 100x/1.46NA PH3 oil immersion (UV) M27 objective. The images were acquired in ZEN 2.3 Blue software using the phase (5 ms exposure), mCherry (Zeiss filter set 43 HE; 150 ms exposure, Zeiss HBO100 mercury bulb illumination using Osram HBO103/W2 bulbs), EGFP (Zeiss filter set 38 HE; 150 ms exposure, Zeiss HBO100 mercury bulb illumination using Osram HBO103/W2 bulbs) and H3342 (60 ms) channels. We performed all washes by centrifuging cells at 800xg for 3 min.

For the haptomonad-like cells, 18 x 18 mm high-performance coverslips thickness No. 1.5H (Zeiss) were sterilized with 100% ethanol for 5 min in a sterile Petri dish, washed twice with 5 ml of M199 media and transferred to 6-well plates. Further washes were performed twice with 2 mL M199. Promastigotes at 5x10^6 cells/mL in 2 mL of M199 medium were added to the coverslips and allowed to differentiate at 28 °C with 5% CO_2 for 24 h (for localization and intensity measurements) or 72 h with the medium being changed every 24 h (for cell body mispositioning assays). The coverslips were washed twice with 2 mL of DMEM, incubated for 5 min with 2 mL DMEM containing 1 μg/mL of Hoechst 33342 and washed twice with 2 mL of DMEM. Washed coverslips were mounted onto a super frost microscope slide with premarked square wells and another coverslip mounted on top. We imaged the adhered live cells using the Zeiss Axio ImagerZ2 upright microscope with the Zeiss 63x/1.4NA PH3 oil-immersion Plan-Apochromat objective and Hamamatsu Flash 4 camera. Z-stacks were acquired on the phase (5 ms), mCherry (150 ms), EGFP (150 ms) and H3342 (60 ms) channels using a voxel size of 0.103 μm x 0.103 μm x 0.25 μm. All the z-stack images were acquired in ZEN 2.3 Blue software and analyzed using Fiji.[40] Quantification of fluorescence intensities of KIAPs in the adhered flagella was based on average intensity projection using nine z-stack slices of 2.25 μm total thickness. Same analysis settings were applied for each comparison group and the figures generated using the QuickFigures plugin in Fiji.[40,42]

Confocal microscopy

For the confocal microscopy of adhered live cells, 1x10^6 cells/mL log phase promastigotes were grown in 2 mL of M199 in the ibidi's μ-dish 35 mm (high glass bottom) culture dishes for 24 h at 28 °C with 5% CO_2. To remove non-adherent cells, the dishes were washed more than five times with fresh M199, prewarmed at RT. The cells were imaged using an inverted Zeiss LSM880 with Airyscan, 100x oil-immersion alpha Plan- Apochromat objective (1.46NA; DIC M27 Elyra), 561nm laser and Physik Instrumente P-737 piezo stage. We acquired confocal z-stack images in super-resolution Airyscan mode using line scanning and the settings previously described.[15] The images were processed in ZEN 2.3 SP1 FP3 Black (release version 14.0) software and analyzed using Fiji.[40] For the quantification of the adhesion plaque size, nine Airyscan-processed z-stack slices of 0.45 μm total thickness were subjected to average intensity projection. These were then binarized in MATLAB (R2023a) and a pixel intensity threshold of 0.5 used to determine the boundaries of the area enclosed by the SMP1 signal. To exclude cell debris, images with a circularity lower than 2 were selected.

Immunofluorescence microscopy

Approximately 1x10^7 log phase promastigotes of C-terminally tagged KIAP2 and N-terminally tagged PFR2 cell lines expressing mNeonGreen fused to 3myc epitope (KIAP2:: 3Myc::mNG and 3Myc::mNG::PFR2) were washed three times with 1 ml of Voorheis modified PBS (vPBS).[43] The cells were resuspended in 100 μL of vPBS and 50 μL of the cell suspension was settled in the pre-marked circular wells on a super frost microscope slide (Thermo Scientific). The parasites were allowed to adhere to the slides for 5 min, then fixed for 10 min with 4% paraformaldehyde (PFA) in vPBS at RT. Unreacted PFA was quenched with 1% glycine in PBS for 5 min at

RT. Whole-cell cytoskeletons of adhered KIAP2::mNG::3Myc and mNG::3Myc::PFR2 promastigotes were prepared by permeabilizing the cells with 1% IGEPAL CA-630 (Sigma; I3021) in PEME for 30 sec. The cells were fixed with methanol for 20 min at -20 °C, washed with PBS for 20 min at RT, and blocked with 1% BSA in PBS for 1 h at RT. The cells were then incubated with 1:200 c-Myc monoclonal antibody (9E10; MA1-980) in PBS containing 1% BSA for 1 h at RT. The cells were washed four times, with 5 min incubation during each wash, and probed with Alexa Fluor 546 goat anti-mouse secondary antibody (Invitrogen) diluted at 1:1000 in 1% BSA in PBS for 1 h at RT. The slides were washed twice with PBS for 5 min each, incubated with 1 μg/mL of Hoechst 33342 in PBS for 5 min, washed once with PBS for 5 min, and mounted with Vectashield mounting medium for imaging. The images were acquired under the phase, mCherry, EGFP and H3342 channels with the Zeiss 63x/1.4NA PH3 oil-immersion Plan-Apochromat objective, as described above.

Negative staining

$1x10^7$ log phase promastigotes of parental and FAZ34 null mutant cell lines were settled on glow-discharged carbon and formvar-coated nickel grids (200 mesh; Agar Scientific), mounted on tweezers, for 2 min at RT. Detergent-extracted cytoskeletons were prepared by inverting the grids onto ~1 mL drop of 1% IGEPAL CA-630 (Sigma; I3021) in PEME for 5 min at RT. The samples were rinsed twice with ~1 mL drops of PEME and fixed with 2.5% glutaraldehyde (EM grade) in PEME for 10 min at RT. Fixed samples were washed twice in drops of PEME (5 min/ wash), transferred to ~1 mL drop of ddH_2O and stained with 1% aurothioglucose in ddH_2O. The grids were allowed to dry, followed by imaging on a Jeol JEM-1400 Flash transmission electron microscope operating at 120 kV. The images were acquired using a OneView 16-megapixel camera (Gatan/Ametek version 3.52.3932.0, Pleasanton, CA).

Immunogold labelling

Detergent-extracted cytoskeletons of approximately $1x10^7$ log phase promastigotes of the parental cells and cell lines expressing KIAP2::mNG and mNG::PFR fused to 3myc epitope (KIAP2::mNG::3Myc and mNG::3Myc::PFR2) were prepared as described above. The samples were fixed with 4% PFA in PEME for 10 min at RT and the unreacted PFA was quenched with 1% glycine in PEME for 5 min at RT. Each grid was transferred to a drop of PEME (50 μL) for 5 min and blocked for 30 min in a 50 μL drop of 1% BSA in PEME. The samples were incubated with c-Myc monoclonal antibody (9E10; MA1-980) diluted at 1:20 in the blocking buffer for 1 h at RT, followed by three consecutive washes in 50 μL drops of the blocking buffer (5 min/wash). Washed samples were probed with goat anti-mouse secondary antibody conjugated to 10 nm gold (Sigma; G7652; 1:50 dilution in the blocking buffer) for 1 h at RT. The grids were then washed by transferring them to three consecutive drops of PEME (~1 mL/drop; 5 min/wash) and fixed with 2.5% glutaraldehyde in PEME for 10 min at RT. Fixed samples were washed twice in drops of PEME (5 min/ wash) and negatively stained with 1% aurothioglucose in ddH_2O. The samples were allowed to dry and imaged on a Jeol JEM-1400 Flash transmission electron microscope operating at 120 kV, equipped with a OneView 16-megapixel camera (Gatan/Ametek version 3.52.3932.0, Pleasanton, CA).

Bioinformatics analyses

The 18S rRNA sequences of various kinetoplastid species that use different adhesion modes were retrieved from TriTrypDB and GenBank. Alignment and phylogenetic analysis of the sequences were implemented in Geneious prime software (v2025.1).[44] Sequence alignment was performed using MAFFT v7.490 with the default parameters.[45,46] A maximum likelihood (ML) tree was constructed with PHYML v3.3.20180621[47] and RAxML (v8.2.11),[48] utilizing the GTR or GTR GAMMA substitution models with default settings. Branch support values were computed based on 1000 bootstrap replicates. The resulting species tree was used to map the presence or absence of FAZ and KIAP proteins in the representative kinetoplastid species. Reciprocal best BLAST searches of the relevant genomes were employed to identify orthologous sequences, with a minimum e-value threshold of 10^5.[49] *L. mexicana* FAZ2, FAZ5, FAZ34 and KIAP1-3 protein sequences were used to query the protein sequence database on TriTrypDB via BLASTP, which identified corresponding sequences in other kinetoplastid species. The top hit protein sequence from each species was subsequently used to query the *L. mexicana* genome by BLASTP. The proteins were considered orthologous if the same *L. mexicana* FAZ or KIAP proteins were returned as the top hit in the subsequent searches.

QUANTIFICATION AND STATISTICAL ANALYSIS

Statistical analysis

The means were calculated in Microsoft Excel and are presented in the results as mean ± S.D along with the exact number of samples analyzed (n). Where appropriate, we have also shown the number of samples or technical replicates analyzed in the figure legends. Statistical differences between groups were estimated using the two-tailed Welch's t-test or the Mann-Whitney test, according to whether or not the data was normally distributed, at $p < 0.05$ significance level in GraphPad Prism (v9.5). Data plots were created using GraphPad Prism.

Current Biology, Volume *35*

Supplemental Information

Discovery of a novel flagellar filament system underpinning *Leishmania* adhesion to surfaces

Barrack O. Owino, Ryuji Yanase, Alan O. Marron, Flavia Moreira-Leite, Sue Vaughan, and Jack D. Sunter

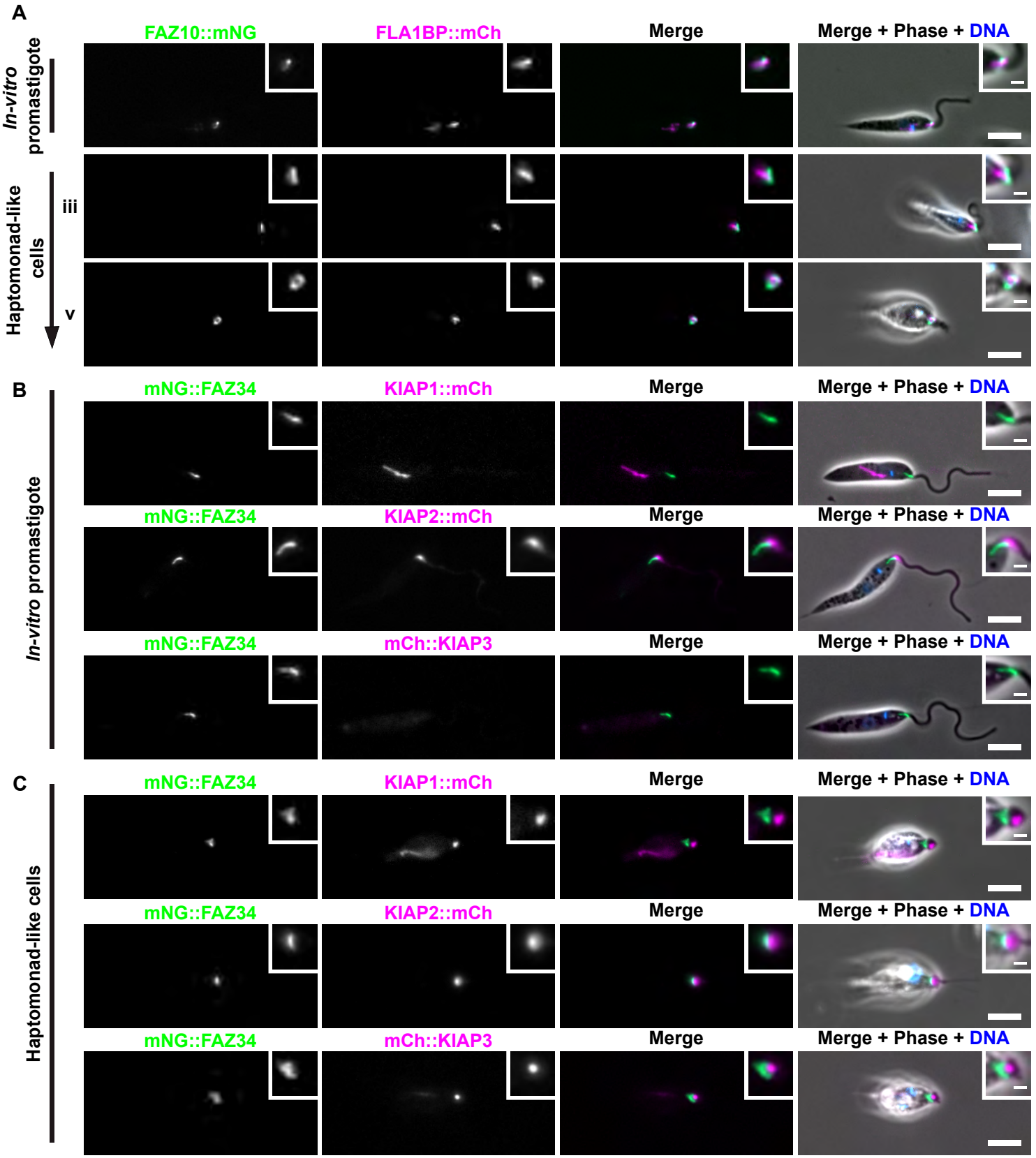

Figure S1. Localisation of FAZ and KIAPs1-3 in *L. mexicana in vitro* promastigote and haptomonad-like cells, Related to Figure 1. (A) Fluorescence micrographs of *L. mexicana* promastigote and haptomonad-like cells expressing mNeonGreen (mNG) and mCherry (mCh) tagged FAZ10 and FLA1BP proteins at stages iii and v of differentiation. Insets illustrate a magnified view of the FAZ signal at the different stages. (B-C) Localisation of mNG-tagged FAZ34 and mCherry-tagged KIAP1, KIAP2 or KIAP3 in *L. mexicana* promastigote (A) and haptomonad-like cells (B). Insets show a magnified view of FAZ34 and KIAPs1-3 signals and the position of FAZ34 relative to KIAPs1-3 in promastigotes and haptomonad-like cells. The nucleus and kinetoplast DNA are shown in blue, following Hoechst 33342 staining. Scale bars: 5 μm, insets: 1 μm.

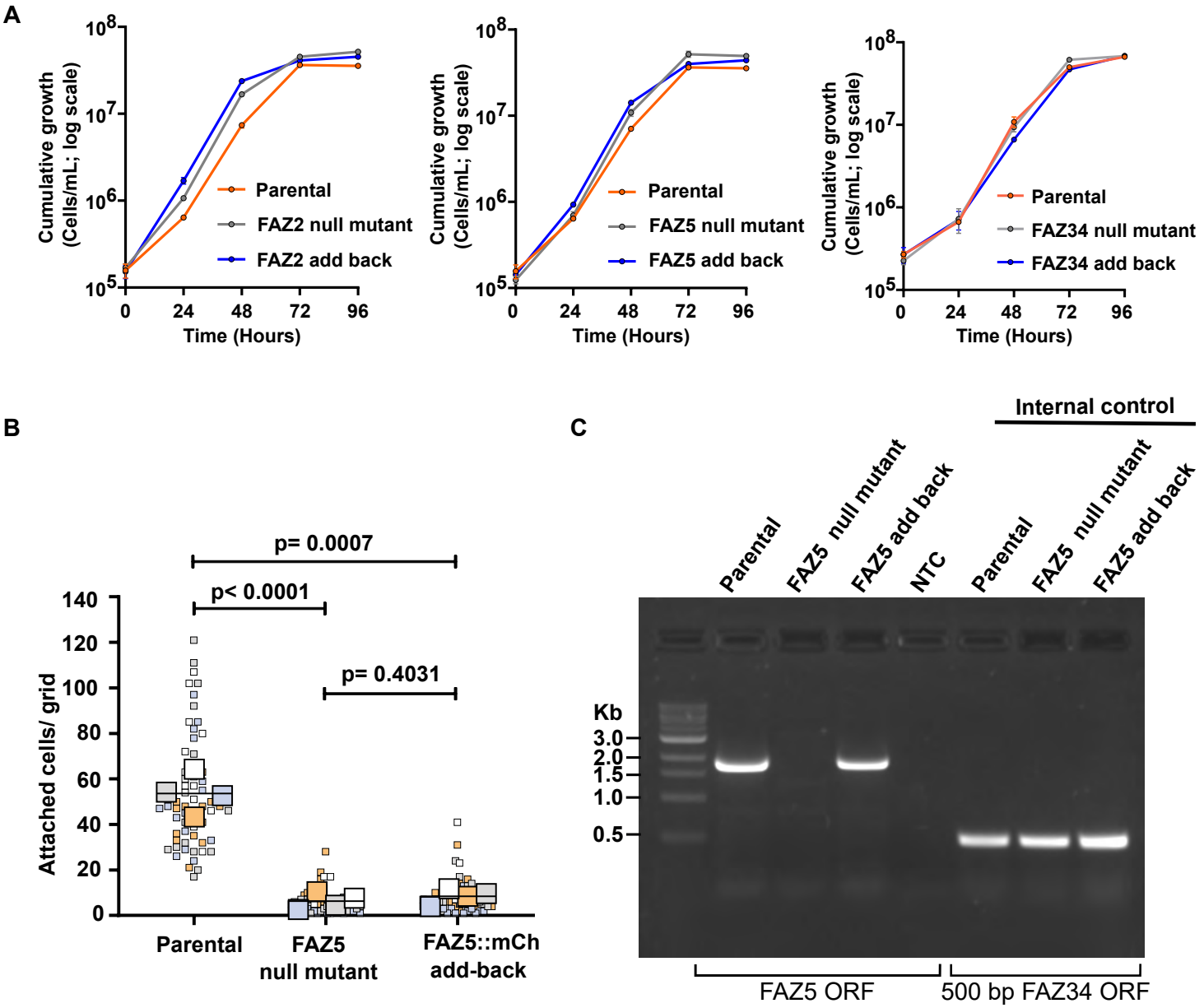

Figure S2. Growth curves, adhesion quantification, and FAZ5 deletion and add-back confirmation, Related to Figure 2. (A) Cumulative growth curves of parental and FAZ2 (left), FAZ5 (middle), and FAZ34 (right) null mutant and add-back cell lines. Data from three independent experiments are shown with the error bars representing the mean ± SD. (B) Quantification of the number of adhered haptomonad-like cells for the parental, FAZ5 null mutant and an add-back cell line in which FAZ5 protein was fused to mCherry. The orange, blue, white and grey colour codes represent measurements from four independent experiments (n = 4), with the small squares indicating individual counts per grid area while the large squares show the average counts per experiment. The horizontal bars represent the overall mean value across the four indipendent experiments. The p-values were calculated using the Welch's two-tailed t-test.(C) Confirmation of deletion and add-back of FAZ5 gene. Genomic DNA from the parental, FAZ5 null mutant and FAZ5 add-back cell lines were analysed by PCR and resolved on 1% agarose gel. We observed a band of ~1.9 Kb, corresponding to the FAZ5 ORF, in the parental and FAZ5 add-back, but not in the FAZ5 null mutant cell line, confirming the successful deletion and add-back of the gene. The successful amplification of ~500 bp FAZ34 internal control in all the cell lines indicated a good quality DNA and efficient PCR amplification. NTC: nuclease-free water

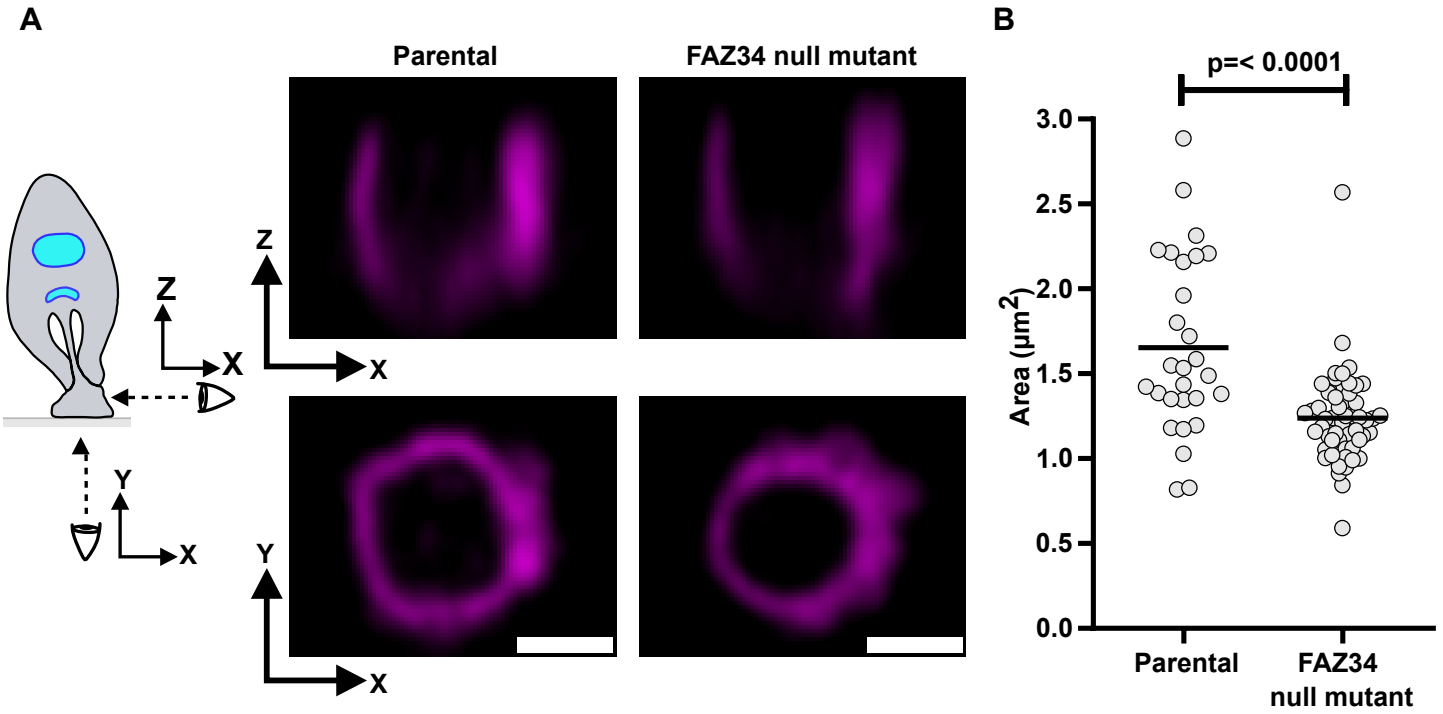

Figure S3. FAZ34 deletion reduced the size of the adhesion plaque, Related to Figure 3. (A) Z-stack confocal microscopy analysis of the adhered flagella of parental and FAZ34 null mutant cells expressing SMP1 endogenously tagged with mCherry. The schematic diagram illustrates the different viewing positions: X-Y (bottom view), and X-Z (side view). Scale bars: 1 µm. (B) Quantification of the area enclosed by the SMP1 signal in the parental (n = 28) and FAZ34 null mutant (n = 54) cells after 72 h of adhesion on glass coverslips. For the area measurements, we binarised the Airyscan-processed images of 0.45 µm thickness in MATLAB (R2023a) and used a 0.5-pixel intensity threshold to determine the boundaries of the area enclosed by the SMP1 signal. To exclude cell debris, images with a circularity lower than 2 were selected. We calculated the p-values using the Mann-Whitney test.

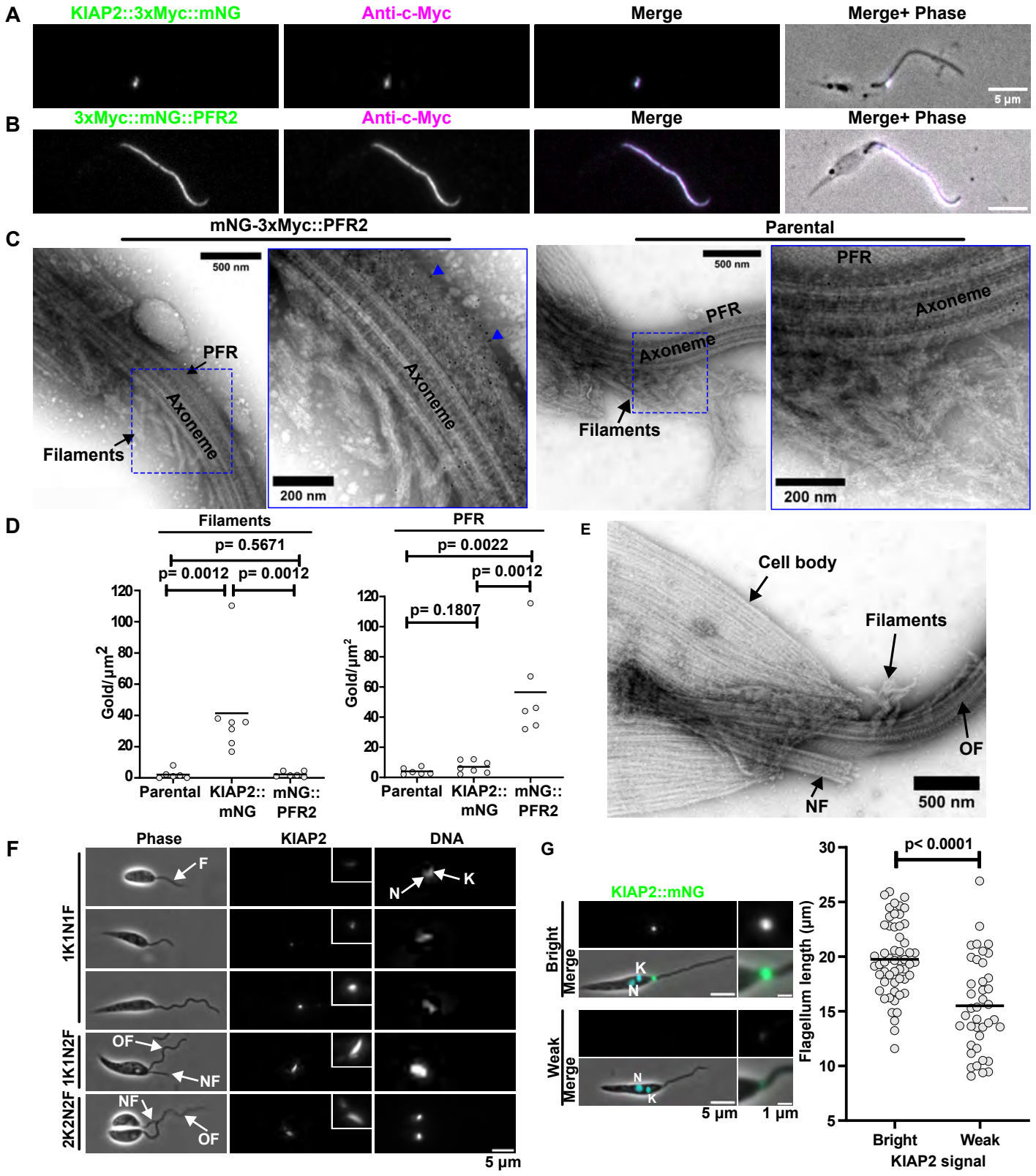

Figure S4. FAZ34 deletion separated KIAP2 and a novel set of filaments from the anterior cell tip in *L. mexicana* promastigote, Related to Figure 4. (A, B) Confirmation of 3Myc::mNG tagged KIAP2 and PFR2 expression in detergent-extracted cytoskeletons of *L. mexicana* promastigotes by immunofluorescence. Scale bars: 5 µm. (C) Immunogold labelling of 3Myc::mNG::PFR2 (positive control) and untagged parental (negative control) cell lines. Insets show a detailed view of the different structures. (D) Quantification of the number of gold particles in the filaments (left) and PFR (right) for the parental, KIAP2::3Myc::mNG and 3Myc::mNG::PFR2 cell lines. Images (parental: n = 6; KIAP2::3Myc::mNG:: n = 7; 3Myc::mNG::PFR2: n = 6) were partitioned into 1 μm^2 grids in Fiji; four complete squares were achieved for each image and the number of gold particles was counted. The horizontal bars represent the mean of gold particles in each structure across the cell lines. P-values were calculated using the Mann-Whitney test. (E) Negatively stained dividing cell showing the presence of the filaments on the old flagellum (OF), but not on the new flagellum (NF). (F) Fluorescence micrographs of major cell cycle stages based on the number of kinetoplasts (K), nuclei (N) and flagella (F). KIAP2 was C-terminally tagged with mNG, while the nucleus and kinetoplast were stained with Hoechst 33342. Insets show a magnified view of the KIAP2::mNG signal. Scale bars: 5 µm. (G) Quantification of KIAP2 signal in 1K1N1F cells (bright: n = 55; weak: n = 40). We calculated the p-values using the Mann-Whitney test.

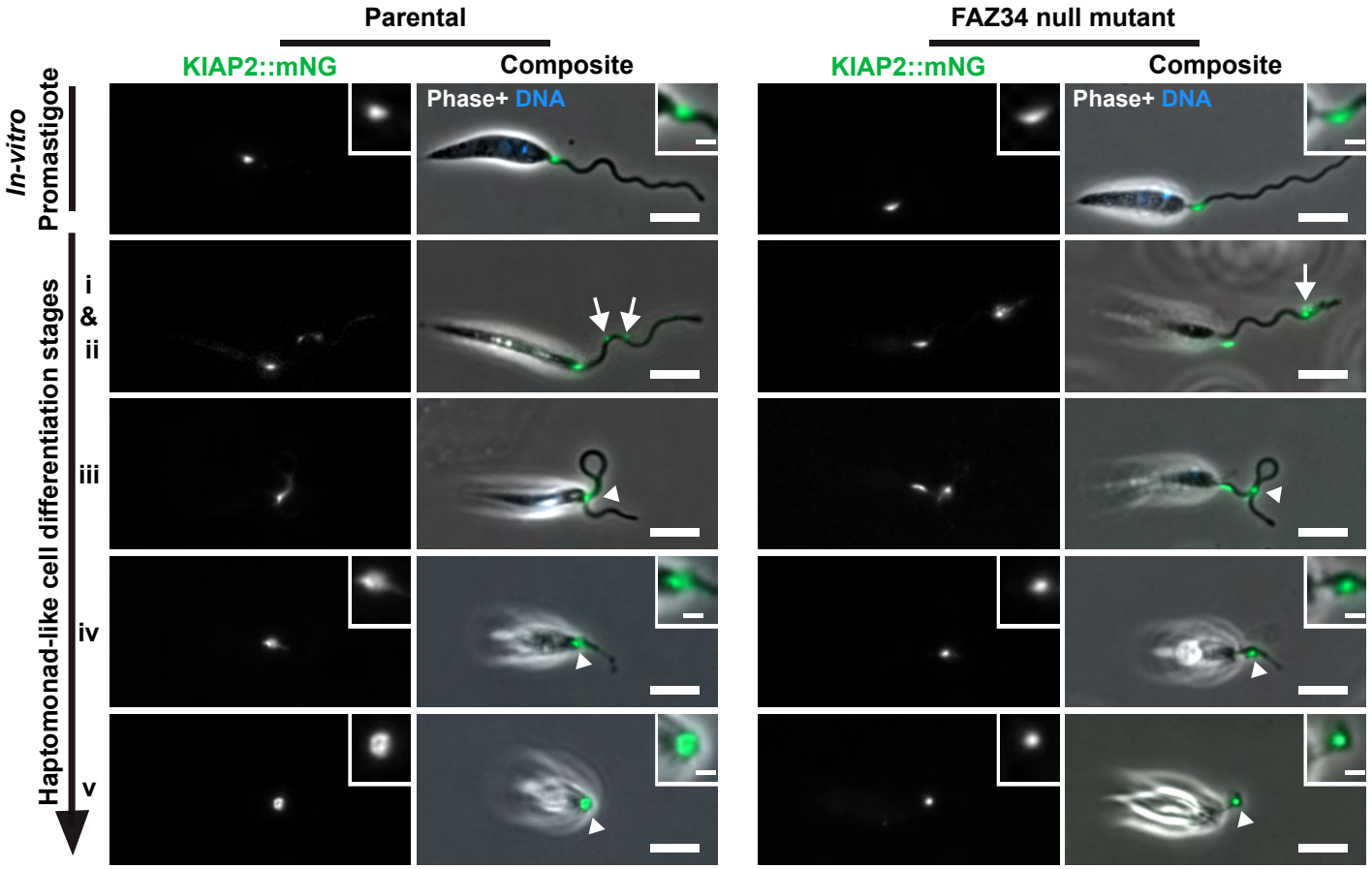

Figure S5. Deletion of FAZ34 separated the cell body from the KIAP2 signal and the adhesion plaque during adhesion of haptomonad-like cells, Related to Figure 5. Development of mNG-tagged KIAP2 in the parental (left) and FAZ34 null mutant (right) *L. mexicana in vitro* promastigotes and haptomonad-like cells. The arrows show bright spots associated with initial foci of adhesion,while the arrowheads denote the position of the adhesion plaque in haptomonad-like cells. The composite shows the phase contrast, KIAP2::mNG (green) and DNA (blue) signals. Scale bars: 5 μm; insets: 1 μm

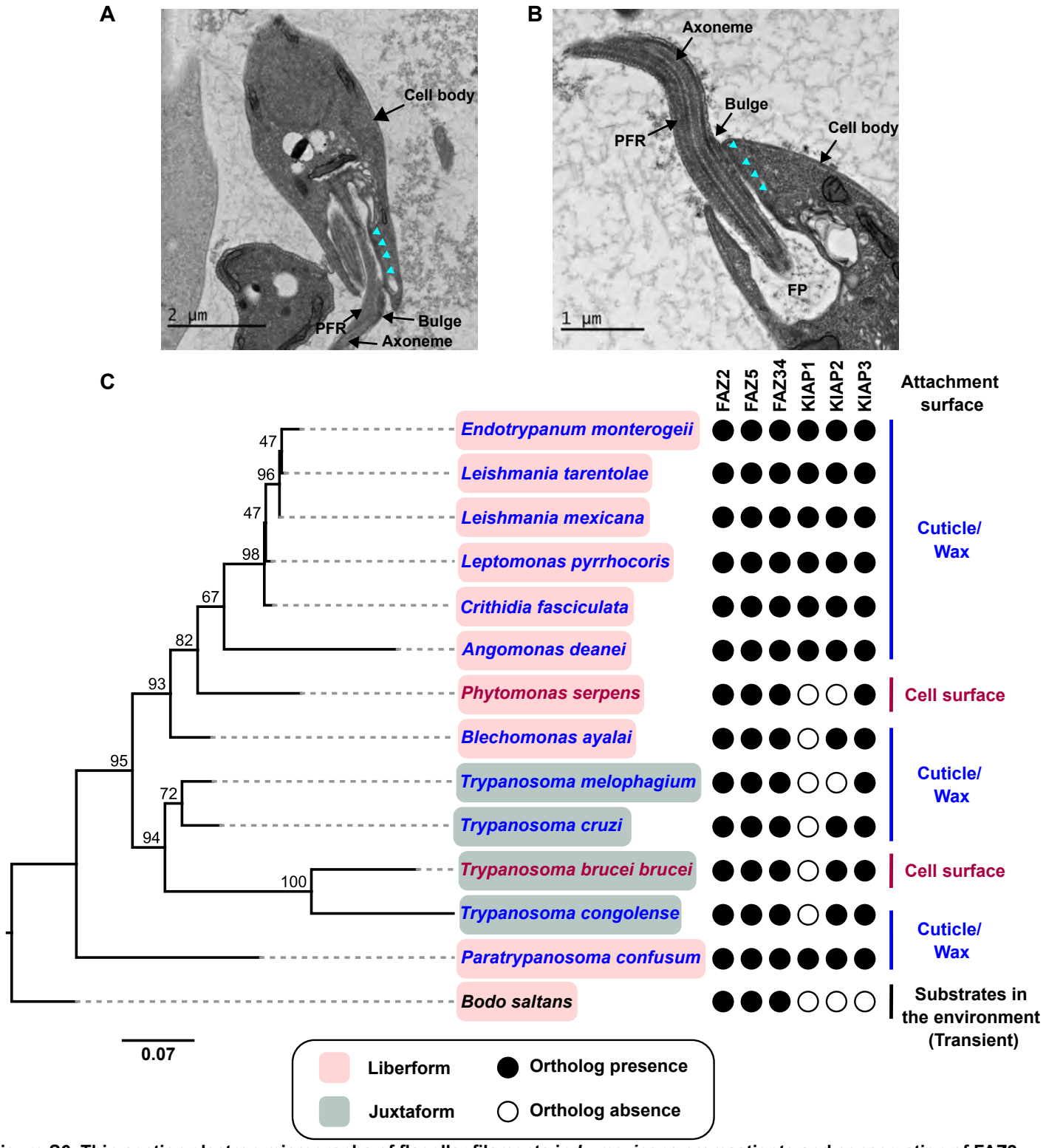

Figure S6. Thin-section electron micrographs of flagellar filaments in *L. mexicana* promastigote and conservation of FAZ2, FAZ5, FAZ34 and KIAP1-3 across kinetoplastids, Related to Figure 4 and Figure 6. (A-B) Transmission electron micrographs of *L. mexicana* longitudinal sections through the flagellum and flagellar pocket showing a bulge on the side associated with the flagellum attachment zone (FAZ; arrowheads), corresponding to the position of the filaments. FP: Flagellar pocket. (C) A phylogenetic tree based on 18S rRNA showing the presence (filled circle) or absence (open circle) of the FAZ proteins and KIAP1-3 across kinetoplastids. The species are highlighted based on the morphological superclass they belong to (i.e. liberform or juxtaform- see graphical legend), with those indicated in blue known to adhere to cuticular or wax layers in their insect vector, while those shown in red are known to adhere to epithelial membranes in the insect vector. Bodo saltans is a free-living kinetoplastid, known to exhibit transient adhesion to substrates in the environment. The species tree was produced using PhyML maximum likelihood analysis with the best-fitting GTR model from an alignment of 2,451 bases. The tree is drawn to scale with the branch lengths representing the number of substitutions per site, while the branch labels indicate percentage bootstrap support values among 1000 replicates. Phylogenetic clusters exhibiting bootstrap support values <70% lack statistically robust support.